

引用格式：刘松岩，张达，杨明建，等，2024. 熊耳山矿集区蒿坪沟 Ag-Au 多金属矿床绿泥石特征及其找矿意义 [J]. 地质力学学报, 30 (1) : 129–146. DOI: [10.12090/j.issn.1006-6616.2023121](https://doi.org/10.12090/j.issn.1006-6616.2023121)

Citation: LIU S Y, ZHANG D, YANG M J, et al., 2024. Characteristics of chlorites from the Haopinggou Ag-Au polymetallic deposit in the Xiong'ershan ore concentration area and its exploration implications[J]. Journal of Geomechanics, 30 (1) : 129–146. DOI: [10.12090/j.issn.1006-6616.2023121](https://doi.org/10.12090/j.issn.1006-6616.2023121)

熊耳山矿集区蒿坪沟 Ag-Au 多金属矿床绿泥石特征及其找矿意义

刘松岩¹, 张 达¹, 杨明建¹, 张鑫明¹, 未国栋¹, 聂胜强¹, 王 轩^{2,3},
冯彦平⁴, 栗文杰⁴, 陈贵兰⁴

LIU Songyan¹, ZHANG Da¹, YANG Mingjian¹, ZHANG Xinming¹, WEI Guodong¹, NIE Shengqiang¹,
WANG Xuan^{2,3}, FENG Yanping⁴, LI Wenjie⁴, CHEN Guilan⁴

1. 中国地质大学（北京），北京 100083;
 2. 中国地质科学院矿产资源研究所，北京 100037;
 3. 北京大学地球与空间科学学院，北京 100871;
 4. 河南发恩德金属矿产有限公司，河南 洛阳 471700
1. *China University of Geosciences, Beijing 100083, China;*
 2. *Key Laboratory of Mineralization and Resource Evaluation, China Institute of Geology and Mineral Resources, Beijing 100037, China;*
 3. *School of Earth and Space Sciences, Peking University, Beijing 100871, China;*
 4. *Henan Found Mining Co., Ltd., Luoyang 471700, Henan, China*

Characteristics of chlorites from the Haopinggou Ag-Au polymetallic deposit in the Xiong'ershan ore concentration area and its exploration implications

Abstract: [Objective] The Haopinggou Ag-Au polymetallic deposit is a typical intermediate-sulfidation epithermal deposit in the Xiong'ershan ore concentration area. Ag-Pb-Zn mineralization mainly occurs in steeply dipping veins and breccia matrix. The relationship between large-scale Pb-Zn mineralization and widely developed alteration minerals remains unclear. [Methods] In order to discuss chlorite's significance related to Pb-Zn mineralization, chlorite composition in the Haopinggou Ag-Au polymetallic deposit has been analyzed by field geological observation and electron microprobe analysis (EMPA) in this paper. [Results] Three types of chlorite were observed in the deposit, occurring in altered wall rocks (Type I), in(with) Pb-Zn sulfides (Type II), and in(with) the breccia matrix (Type III). All three types of chlorite are prochlorites and fall within the compositional range of Fe-rich chlorite, indicating that they could be formed in a partially reducing acidic environment. Fe²⁺ for Mg²⁺ is the primary substitution in chlorite lattice, suggesting a close association between chlorite formation and mafic wall rocks. Based on the corrected chlorite geothermometer, these chlorites formed under aluminum-saturated conditions in the medium to low-temperature range of 196–239°C. The temperatures of chlorites associated with mineralization (Types II and III) are higher than those in chlorites around quartz veins (Type I). It is believed that during the mineralization process, the hydrothermal fluids evolved from acidic to nearly neutral conditions as the temperature gradually decreased. The initial acidic environment facilitated interaction between water and rocks,

基金项目：校企合作项目（No. 33112021007）；国家自然科学基金（422020067）

This research is financially supported by the School-Enterprise Cooperation Project (Grant No. 33112021007) and the National Natural Science Foundation of China (Grant No. 42202067).

第一作者：刘松岩（1996—），男，在读博士，构造地质学专业。Email: 380126504@qq.com

通讯作者：张达（1967—），男，教授，主要从事构造地质学与区域成矿规律研究。Email: zhangda@cugb.edu.cn

收稿日期：2023-07-25；修回日期：2023-10-18；录用日期：2023-11-02；网络出版日期：2024-01-31；责任编辑：吴芳

promoting the dissolution of surrounding rocks and providing space for the further precipitation of metal sulfides. The evolution of ore fluid properties also corresponds to the deposition process of Ag-Pb-Zn. The genesis of chlorite in the deposit is well-correlated with the ore-forming and holds significant prospecting value. (1) Type I chlorites mainly develop on both sides of quartz veins, formed by the dissolution and metasomatism of basic wall rocks by ore-bearing hydrothermal fluids. Type I chlorite's Fe and Mg components are mostly derived from the wall rocks. Although this type does not contain mineralization, it can be used to trace veins. (2) Type III chlorites reflect the migration process of ore-bearing hydrothermal fluids carrying dissolved minerals (biotite/clinopyroxene), which precipitate with changes in the physicochemical environment. Type III chlorite's Fe and Mg components are mainly introduced by ore-bearing hydrothermal fluids. This type of chlorite fills the intergranular pore spaces between minerals and easily replaces minerals such as biotite and hornblende, exhibiting apparent mineral alteration features in hand specimens, which is beneficial for prospecting.(3) The formation mechanism of Type II chlorites includes the possibilities mentioned above. This type of chlorite is formed by complete dissolution and metasomatism of cement in ore-bearing hydrothermal fluids, forming fine-grained cryptocrystalline chlorite fillings in breccia rocks. Ore-bearing hydrothermal fluids and wall rocks both contribute Fe and Mg in the chlorites. Hand specimens of Type II chlorite are dark green, disseminated and filled in the matrix, making it easy to distinguish. The chemical characteristics of Type II chlorites are similar to those of chemical characteristics of granite-related deposits, implying the contribution of magmatic fluids to ore-forming fluids. [Conclusion] The Haopinggou Ag-Au polymetallic deposit contains three types of chlorites. Their chemical characteristics all reflect an acidic and reducing metallogenic environment. In cation exchange, the primary substitution is Fe for Mg, and other substitutions are insignificant. The effect of Fe/(Fe+Mg) must be eliminated in order to calculate the temperature of such deposits using chlorite geothermometers. The formation mechanism of the three chlorites is closely related to mafic wall rock, and their chemical properties suggest the involvement of magmatic fluids in ore-forming fluids. [Significance] These three types of chlorite are well-matched with intense Ag-Pb-Zn mineralization and can serve as key indicators for locating Pb-Zn veins.

Keywords: Polymetallic deposit; prospecting significance; Chlorite; EMPA; mineralization; Geochemistry; Xiong'ershan.

摘要：为理清蒿坪沟 Ag-Au 多金属矿床中多阶段矿化与热液蚀变之间的关系，文章选取与铅锌成矿阶段密切相关的绿泥石进行野外观察及电子探针分析。文章将蒿坪沟 Ag-Au 多金属矿床中的绿泥石分为 3 类：I 型分布在石英脉两侧的围岩中；II 型呈细粒、隐晶质填充于隐爆角砾岩基质；III 型与铅锌硫化物共生、或以蠕虫状广泛分布在石英颗粒间隙中。3 种类型绿泥石均为斜绿泥石，并落在了铁镁绿泥石的范围内，指示其形成于偏还原的酸性环境中；在阳离子置换中，主要发生了 Fe^{2+} 对 Mg^{2+} 的置换，其余置换作用均不明显；3 种绿泥石形成与镁铁质围岩关系密切。由校正后的绿泥石地质温度计估算出 3 种类型绿泥石的形成温度为 196~239 °C，属于中—低温热液蚀变范围。3 类绿泥石与蒿坪沟 Ag-Au 多金属矿床银铅锌成矿阶段相匹配，对进一步找矿勘查具有重要意义。绿泥石化学特征表明岩浆热液参与了成矿流体的形成，绿泥石形成于熊耳山矿集区早白垩世大规模岩浆—成矿时期。

关键词：多金属矿床；找矿；绿泥石；电子探针；成矿；地球化学；熊耳山

中图分类号：P614 文献标识码：A 文章编号：1006-6616（2024）01-0129-18

DOI: [10.12090/j.issn.1006-6616.2023121](https://doi.org/10.12090/j.issn.1006-6616.2023121)

0 引言

绿泥石属于结构为 2:1:1(也记作 TOTO)的层状镁、铁铝硅酸盐矿物，通常是热液蚀变作用的标志产物，与金、铜和铀等矿床密切相关(Lowell and Gilbert, 1970; Cathelineau and Nieva et al., 1985; Pacey et al., 2020)。绿泥石可以稳定存在于较宽的温度范围内，且其成因矿物学特征能反映流体性质和

水—岩反应环境，因此备受矿床学家的重视(Laird, 1988; 郑伟等, 2013; Bourdelle and Cathelineau, 2015; 戴朝成等, 2017; Zhang et al., 2022)。绿泥石的化学成分和晶体结构在不同的成矿环境中呈现规律性的变化，常用的通式为 $(\text{R}_x^{2+}\text{R}_y^{3+}\square_{6-x-y})^{\text{IV}}_6(\text{Si}_z\text{R}_{4-z}^{3+})^{\text{IV}}_4\text{O}_{10}(\text{OH})_8$ ，其中 R^{2+} 代表二价阳离子， R^{3+} 代表三价阳离子， \square 代表八面体空位(Zane and Weiss, 1998)；伴随 3 种主要的阳离子替换：① $\text{Fe}^{2+} \leftrightarrow \text{Mg}^{2+}$ ，② 契尔马克替换 $\text{Al}^{\text{IV}}\text{Al}^{\text{VI}} \leftrightarrow \text{Si}(\text{Mg}^{2+}, \text{Fe}^{2+})$ ，③ 二八—三八面体替换

$3(\text{Mg}^{2+}, \text{Fe}^{2+}) \leftrightarrow \square + 2\text{Al}^{\text{VI}}$ 。结构的多变性表明绿泥石对成矿时期的温度、压力和全岩成分环境非常敏感 (Inoue, 1995; Inoue et al., 2009; Bourdelle et al., 2013), 因此常作为一种重要的标型矿物, 用来揭示金属矿床的成矿作用(刘燚平等, 2016; 方维萱等, 2017; 张娟等, 2021; Zhang et al., 2022)。针对形成温度与绿泥石结构转换之间的关系, Cathelineau and Nieva(1985)根据绿泥石 Al^{VI}含量与温度之间的良好线性关系拟合提出了经验性绿泥石温度计(或铝成分温度计), 后经其他学者校正, 衍生出了一系列计算绿泥石形成温度的线性公式(Cathelineau, 1988; Jowett, 1991; Zane and Fyfe, 1995)。迄今为止, 经验性绿泥石温度计在矿床研究方面运用广泛(王小雨等, 2014; Dora and Randive, 2015; 周栋等, 2018; 葛祥坤等, 2020; Zhang et al., 2022), 但针对不同种类的矿床其适用性还存在较多争议(刘燚平等, 2016)。

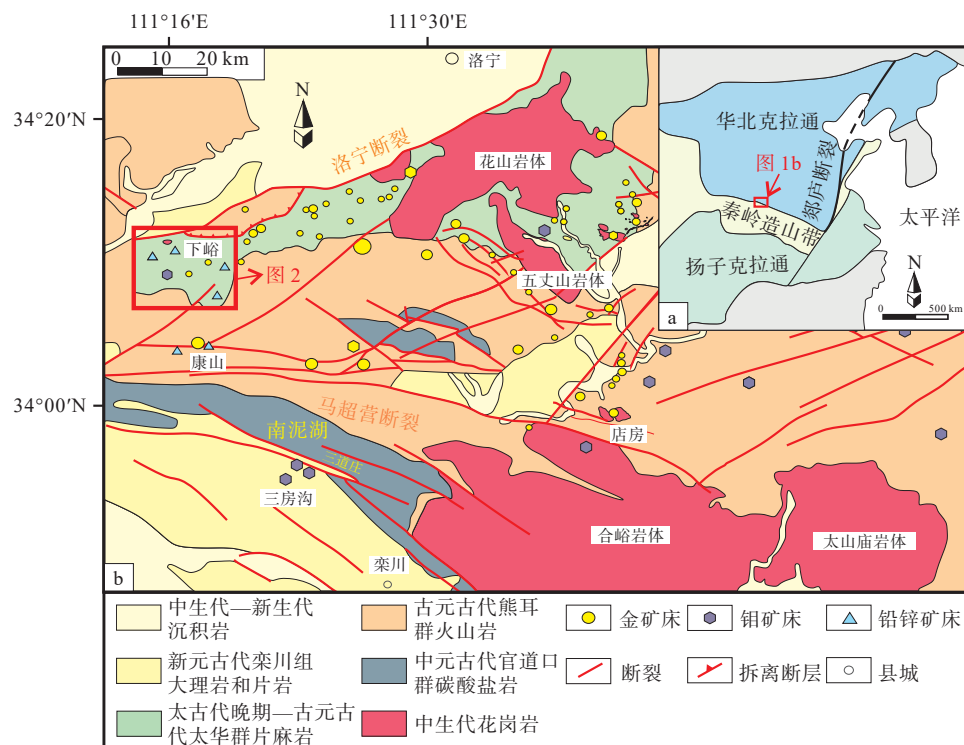
蒿坪沟 Ag-Au 多金属矿床位于华北克拉通南缘熊耳山矿集区西部下峪矿田内, 属东秦岭成矿带中少见的角砾岩-斑岩-浅成低温 Au 多金属矿床 (Tian et al., 2023)。依据原生硫化物组合的硫化状态的“三分法”方案(Hedenquist et al., 2000), 蒿坪沟 Ag-Au 多金属矿床又可归类为中硫型(Sillitoe and Hedenquist, 2005; Tian et al., 2023)。已有研究将该矿床成矿过程大致划分为 3 个阶段: 金-石英-菱铁矿阶段、石英-铅锌硫化物阶段、石英-碳酸盐阶段(陈衍景等, 2003; 程广国, 2013; Li et al., 2013; 徐进鸿, 2021; Tian et al., 2023)。Li et al.(2016)认为金-石英-菱铁矿阶段与陆-陆碰撞过程中碳酸盐-页岩-燧石建造变质脱水有关, 石英-硫化物阶段则以富集银的铅锌矿化为主, 与晚中生代岩浆事件有关。Tian et al.(2023)通过与铅锌同成矿期独居石和磷钇矿年龄范围 $125.7 \pm 1.8 \sim 123.3 \pm 1.7$ Ma 对成矿时代进行了限定, 成矿与同期次的花岗斑岩有关。成矿流体总体被认为属中一低温、中一低盐度流体(陈衍景等, 2003; Chen et al., 2004; 高建京等, 2010; Li et al., 2013; Han et al., 2014; 徐进鸿, 2021), 主成矿期和成矿晚期具有大气水混合的特征(Li et al., 2016; 徐进鸿, 2021)。已有的研究成果对蒿坪沟 Ag-Au 多金属矿床多期多阶段的成矿过程进行了限定, 但并未深入探讨矿化阶段产生的大规模热液蚀变矿物(Li et al., 2013; Tian et al., 2023), 导致矿化过程与热液蚀变矿物之间的关系尚不明确, 一定程度上制约了对矿床成因认识的深化(吕志成等, 2022; 袁航等,

2022)。作为蒿坪沟 Ag-Au 多金属矿床中重要的蚀变矿物, 绿泥石较为完整地记录了蚀变及矿化过程, 对其开展成分及结构研究可以反演银铅锌成矿作用过程。基于野外地质调查, 显微镜下观察和电子探针分析, 文章对蒿坪沟 Ag-Au 多金属矿床中绿泥石的类型、组分、形成温度、环境及形成机制进行了系统研究, 以期约束蒿坪沟 Ag-Au 多金属矿床成矿流体的演化特征及银铅锌沉淀的物理化学环境, 并对成矿期流体性质和绿泥石形成机制进行了初步探讨, 从而为探讨矿床成因及找矿勘查工作提供新的思路与线索。

1 地质背景

熊耳山矿集区地处华北克拉通南缘, 位于华北地台与秦岭造山带的结合部(图 1a), 经历了太古代陆核形成与增生、元古代大陆裂解与俯冲拼贴、古生代陆陆碰撞及中生代陆内活动等重要地质演化过程, 形成了多阶段构造-岩浆-成矿格局(陈衍景等, 2003; Chen et al., 2004; 李诺等, 2008; Mao et al., 2010; Dong et al., 2016; Li et al., 2018; 张国伟等, 2019; Wang et al., 2021)。熊耳山矿集区南部以近东西走向的马超营断裂为界, 北部以洛宁断裂为界, 拆离断层主要位于太华群与熊耳群之间(图 1b)。整个矿集区东西长约 80 km, 南北宽 15~40 km, 面积约 2000 km²。

熊耳山矿集区出露地层单元简单, 主体分为上下两套(Li et al., 2013; 唐克非, 2014)。下部为前寒武纪的结晶基底, 由太华群角闪岩、TTG 片麻岩和富钾片麻岩组成(第五春荣等, 2007; Diwu et al., 2014; Wang et al., 2020); 上部为不整合覆盖于基底之上的盖层, 包括古元古代熊耳群火山岩、中一新元古代官道口群碳酸盐岩(Zhao et al., 2005; Wang et al., 2010)。洛宁断裂为生长正断层, 控制了新生代盆地的分布。北倾的马超营断裂在古生代和中生代活动, 伴生一系列次级北东向陡倾左旋断裂系统, 为熊耳山矿集区主干控矿构造(图 1b; 张元厚等, 2006; Han et al., 2009)。燕山期花岗岩在区内广泛分布, 侵入于太华群片麻岩和熊耳群火山岩中, 岩体产状及成因类型多样, 与熊耳山矿集区晚中生代大规模成矿作用具有密切联系(毛景文等, 2009; Mao et al., 2010; Wang et al., 2015; Li et al., 2015, 2018; Yang et al., 2019; Zou et al., 2019; Hu et al.,



a—华北克拉通南缘在中国东部的位置; b—熊耳山矿集区大地构造简图及矿产分布图

图 1 华北克拉通南缘熊耳山矿集区地质简图 (底图据 Tian et al., 2023 修改)

Fig. 1 Simplified geological map of the Xiong'ershan ore concentration area along the southern margin of the North China Craton (Base map modified after Tian et al., 2023)

(a) The inset showing the tectonic location of the southern margin of the North China Craton in eastern China; (b) Geological map of the Xiong'ershan ore concentration area, showing the distribution of the major deposits

2020)。熊耳山矿集区晚中生代发育大规模脉状金、银铅锌矿床, 同时伴有一定规模的斑岩型和隐爆角砾岩型金矿化。金矿床主要以石英脉型、蚀变岩型和角砾岩型为主, 银铅锌矿床则以陡倾多金属硫化物脉的形式产出。

2 矿床地质

蒿坪沟 Ag-Au 多金属矿床位于熊耳山矿集区下峪矿田的西北部(图 1b), 与后张沟 Ag(Cu)矿床、沙沟 Ag-Pb-Zn 矿床、铁炉坪 Ag-Pb(Cu)等矿床相邻(图 2)。矿区主要发育脉状 Ag-Au 多金属矿体, 局部可见赋存于隐爆角砾岩体中的矿化。总体上, 该矿床累计查明银 270 t、铅锌 80000 t、金 3000 kg。

蒿坪沟 Ag-Au 多金属矿床出露地层主要为太华群(Arth)片麻岩, 矿床区北部被熊耳群(Pt_{2x})火山岩及新生代沉积岩覆盖(图 2)。矿区内断裂构造发育, 以北东向为主, 其次为近南北向和北北东向。矿床区西北部有晚中生代花岗斑岩出露, 面积约 0.1

km², 其与蒿坪沟 Ag-Au 多金属矿床成矿关系密切。根据已有研究统计, 花岗斑岩锆石 U-Pb 年龄共分为 3 期(~ 135 Ma, ~ 123 Ma, ~ 110 Ma; 叶会寿, 2006; Mao et al., 2011; 梁涛等, 2015; 刘文毅等, 2019; Tian et al., 2023)。北西走向的隐爆角砾岩体位于花岗斑岩的南东部(图 2), 长约 750 m, 宽约 50~130 m, 为蒿坪沟 Ag-Au 多金属矿床内的主要赋矿地质体, 热液矿物主要赋存于基质中, 其矿化阶段和矿物组合与陡倾矿脉一致(Tian et al., 2023)。

根据蒿坪沟 Ag-Au 多金属矿床探矿及采矿成果(图 3), 铅锌矿体主要分布在矿区内的二十多条断裂带内, 矿脉以陡倾斜为主, 倾向多为北西向, 脉宽 0.3~5.7 m 之间; 矿体严格受断裂构造带控制, 呈现明显的分支复合、膨大缩小现象, 走向及倾向上多呈舒缓波状。矿体以脉状、透镜状为主, 总体表现为“伸展脉”的特征(Li et al., 2013)。蒿坪沟 Ag-Au 多金属矿床矿石矿物主要为方铅矿、闪锌矿及含银硫化物, 脉石矿物为石英、铁白云石和菱铁矿。矿石构造主要以脉状、网脉状及角砾状为主。

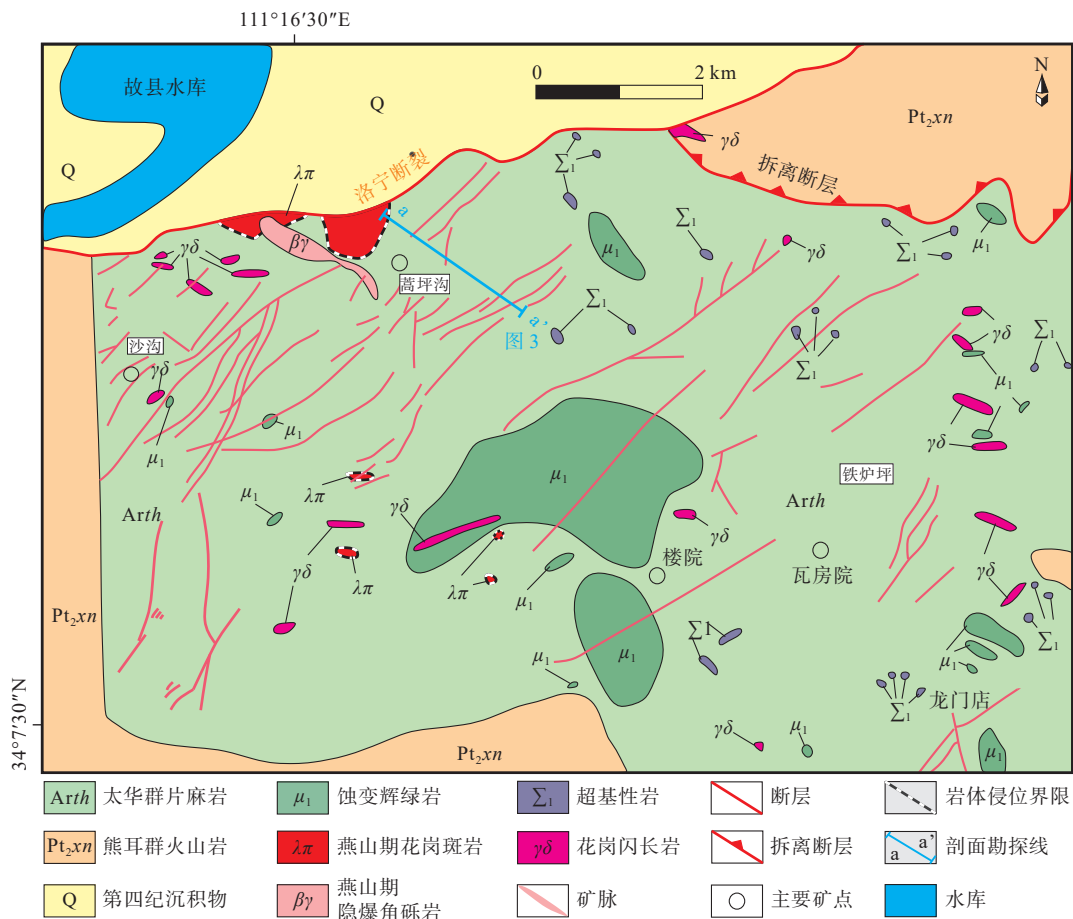


图 2 蒿坪沟 Ag-Au 多金属矿床地质简图 (底图据梁涛等, 2015 修改)

Fig. 2 Geological map of the Haopinggou Ag-Au polymetallic deposit (Base map modified after Liang et al., 2015)

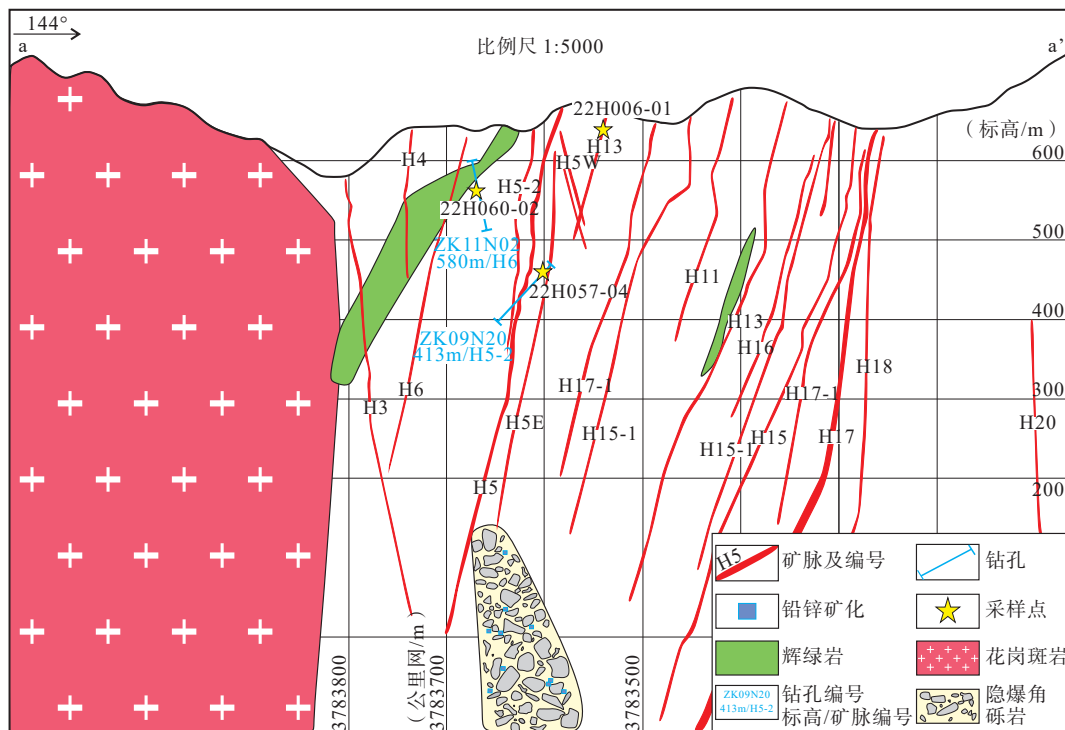


图 3 蒿坪沟 Ag-Au 多金属矿床勘探线剖面图 (剖面位置见图 2)

Fig. 3 Representative cross-section of the Haopinggou Ag-Au polymetallic deposit (The position of the cross-section is shown in Fig. 2.)

结合已有研究成果,蒿坪沟 Ag-Au 多金属矿床成矿过程可以划分为 3 个阶段;从早到晚分别为阶段 I:石英-菱铁矿-黄铁矿阶段,阶段 II:石英-方铅矿-闪锌矿阶段,阶段 III:石英-碳酸盐阶段(图 4; Li et al., 2013; Tian et al., 2023)。

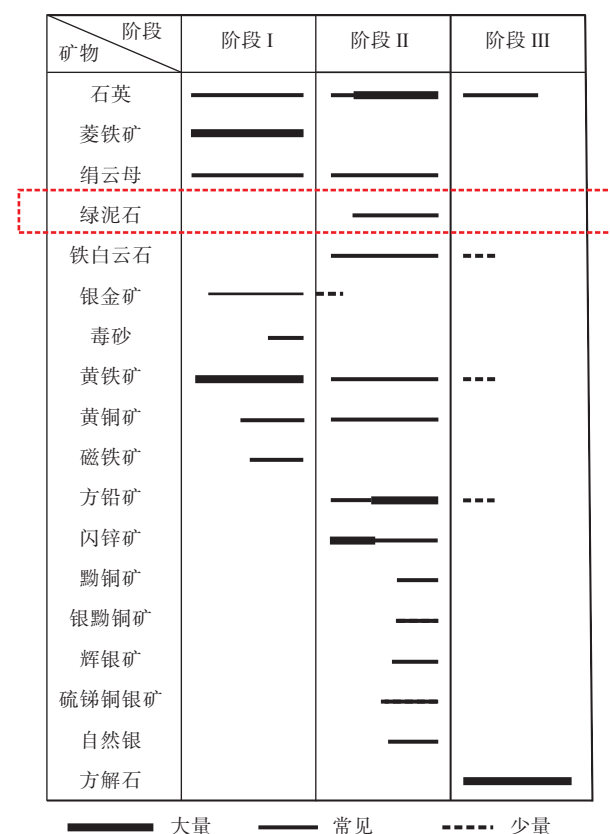


图 4 蒿坪沟 Ag-Au 多金属矿床矿物共生序列(据 Tian et al., 2023 修改)

Fig. 4 Paragenetic sequence of the Haopinggou Ag-Au polymetallic deposit(modified after Tian et al., 2023)

蒿坪沟 Ag-Au 多金属矿床围岩蚀变普遍发育,类型多样。通过收集巷道和钻孔中采集的矿化和蚀变样品,对其矿物组合和结构关系进行了统计和观察。矿脉与围岩接触界线截然,蚀变矿物常形成对称的蚀变晕,宽度在 0.2~2m 之间。整体而言,蚀变带由内向外通常为绢云岩化(最常见)→泥质→青磐岩化,分别对应的矿物组合为绢云母(伊利石)-石英±碳酸盐,高岭石-蒙脱石以及绿泥石-阳起石±绿帘石±碳酸盐(Tian et al., 2023)。绿泥石是蒿坪沟 Ag-Au 多金属矿床中很重要的热液蚀变矿物,在片麻岩围岩、陡倾矿脉及隐爆角砾岩中都有分布,尤其是在矿化强烈的部位,绿泥石十分发育(图 5a)。根据已有成果显示及实地野外观察,绿泥

石的发育与石英铅锌矿脉具有共生/伴生关系(图 5a; Tian et al., 2023),可以用来反映该期热液流体的物理化学环境。

3 样品及研究方法

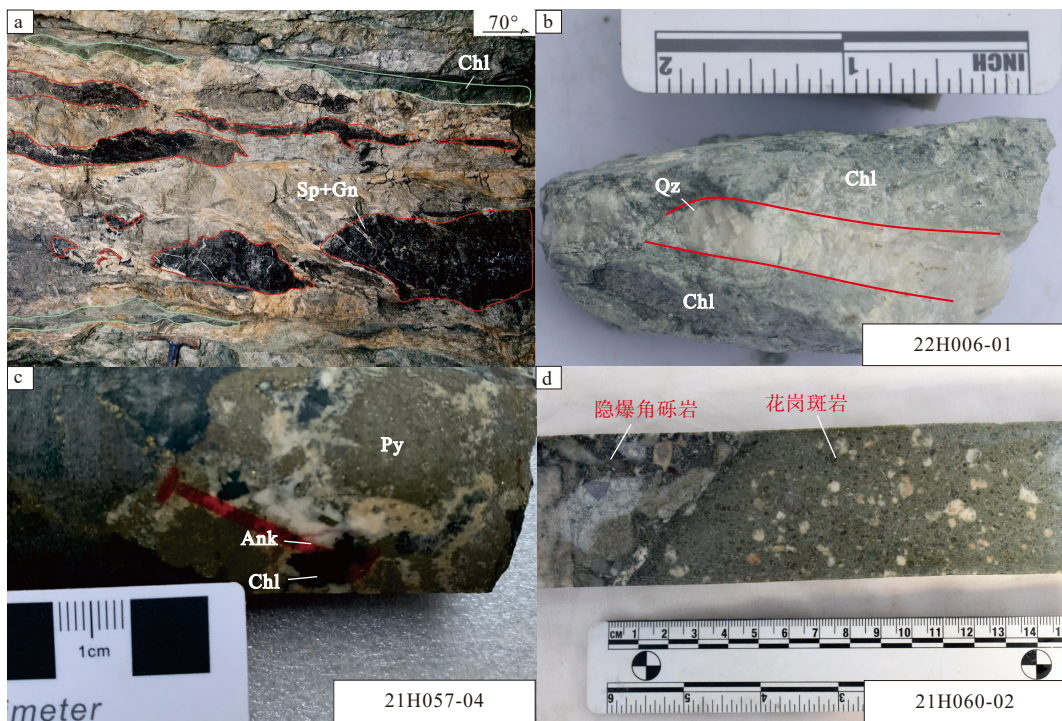
通过系统采集含矿石英脉和隐爆角砾岩中的样品,并开展野外观察和室内镜下鉴定,将蒿坪沟 Ag-Au 多金属矿床中的绿泥石划分为 3 种类型,明确了不同类型矿物形态、分布位置和组合特征。具体样品采集位置及矿物组合如下:①样品 22H006-1 采自 740 中段 H13 号脉附近,可见(I型)绿泥石分布在石英-方铅矿脉体的两侧围岩(图 5b);②样品 21H57-04 采自钻孔 ZK09N20 大约孔深 7.1m 处,可见(II型)绿泥石以细粒隐晶质形式充填于隐爆角砾岩基质,与铁白云石共生(图 5c);③样品 21H60-02 取自钻孔 ZK11N02 孔深 242.3 m,其中斑岩角砾发生蚀变,可见基质中(III型)绿泥石与闪锌矿及黄铁矿共生(图 5d)。

根据样品分布及矿物组合特征(图 6a—6d),进一步开展了电子探针分析。由于绿泥石颗粒细小,结构复杂,多含有其他矿物的微细包裹体,为提高数据精确性和可信度,每件样品采取多区域分散取点,每个区域选取 6~8 个点,避免数据偶然性,选点过程中避开裂隙及矿物包裹体,在 BSE(背散射光)下尽量选取平整、光滑的绿泥石表面(图 6e—6f)。

绿泥石的化学成分分析在河北省廊坊地质调查研究院电子探针实验室完成,测试仪器型号为 JEOL EPMA8230,加速电压 15 kV,加速电流 20 nA,束斑直径 5 μm。标样采用天然矿物或者合成金属国家标准,分析误差小于 0.01%。

4 绿泥石的化学成分特征

通常认为绿泥石电子探针数据中 $(\text{NaO}+\text{CaO}+\text{K}_2\text{O}) < 0.5\%$ 可以排除混染对绿泥石的影响(Hillier, 1993; Zane and Fyfe, 1995)。蒿坪沟 Ag-Au 多金属矿床绿泥石样品数据中 $(\text{NaO}+\text{CaO}+\text{K}_2\text{O})$ 均小于 0.5,可以用来讨论绿泥石的化学特征。Dyar et al. (1992) 认为除了少部分极端氧化环境外,绿泥石 Fe^{3+} 的含量都很低,因此可以使用全铁代表 Fe^{2+} 的含量。手标本及镜下观察表明 I 型绿泥石为深绿色(图 5, 图 6),以脉状或叶片状分布于含铅锌矿石英脉两侧。电



Chl—绿泥石; Gn—方铅矿; Sp—闪锌矿; Py—黄铁矿; Ank—铁白云石
a—铅锌矿脉两侧围岩绿泥石蚀变; b—石英脉两侧蚀变绿泥石; c—隐爆角砾岩基质中填充绿泥石与铁白云石; d—隐爆角砾岩中发生绿泥石蚀变的斑岩角砾

图 5 蒿坪沟 Ag-Au 多金属矿床绿泥石分布情况

Fig. 5 Distribution of chlorites in the Haopinggou Ag-Au polymetallic deposit

(a) Chlorite alteration of surrounding rocks on both sides of Pb-Zn veins; (b) Altered chlorites occurred on both sides of quartz veins; (c) Chlorites and ankerites filled in breccia matrix; (d) Chlorite-altered porphyry breccia
Chl—chlorite; Gn—galena; Sp—sphalerite; Py—pyrite; Ank—ankerite

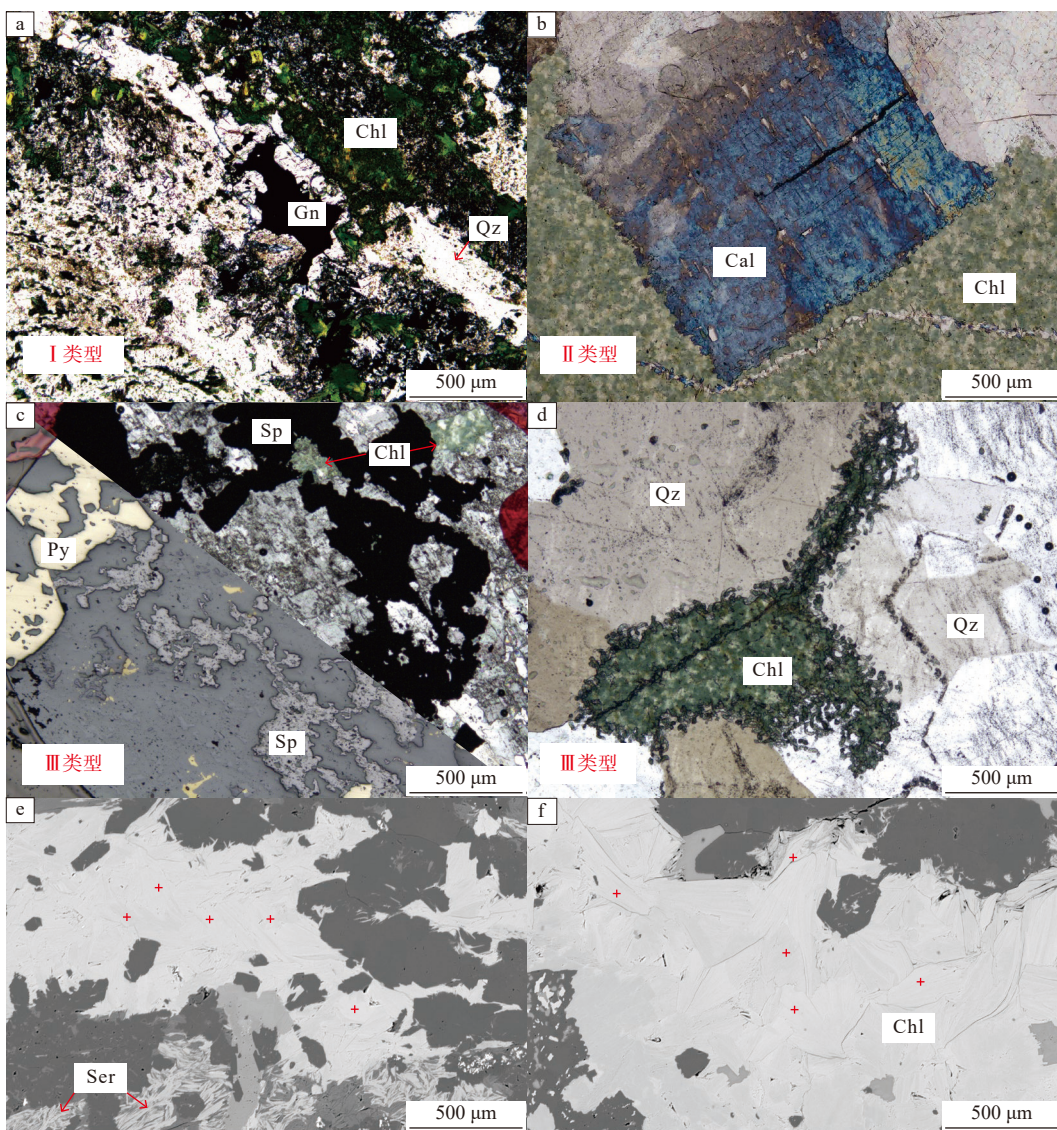
子探针数据显示 I 型绿泥石中 SiO_2 含量集中于 25.54%~31.84%, 均值为 26.71%; Al_2O_3 含量范围为 13.37%~17.61%, 均值为 14.41%; FeO 含量集中于 32.93%~39.36%, 均值为 36.99%; MgO 含量范围为 6.42%~9.45%, 均值为 7.84%。

II 型绿泥石在手标本下为墨绿色, 显微镜下为浅绿色, 呈浸染状填充于隐爆角砾岩基质中。电子探针数据显示 SiO_2 含量集中于 25.52%~26.51%, 均值为 26.03%; Al_2O_3 含量范围为 14.09%~15.68%, 均值为 15.27%; FeO 含量集中于 32.61%~34.23%, 均值为 33.30%; MgO 含量范围为 8.82%~9.42%, 均值为 9.22%。

III 型绿泥石在手标本中呈灰绿色, 显微镜下为翠绿色, 以蠕虫状分布于石英颗粒间隙; 电子探针数据显示 SiO_2 含量集中于 26.65%~29.45%, 均值为 27.17%; Al_2O_3 含量范围为 13.55%~15.90%, 均值为 15.19%; FeO 含量集中于 30.86%~33.33%, 均值为 32.11%; MgO 含量范围为 10.93%~14.31%, 均值为

11.75%。

通过电子探针数据(实验数据在 OSID 码中)可计算 3 种类型绿泥石的结构特征, 其中 I 型绿泥石八面体二价阳离子数为 $\text{R}^{2+}=6.11\sim 7.12$, II 型为 $\text{R}^{2+}=6.81\sim 6.94$, III 型为 $\text{R}^{2+}=6.45\sim 6.74$; I 型绿泥石八面体空位为 $\square=0\sim 0.06$, II 型为 $\square=0\sim 0.05$, III 型为 $\square=0\sim 0.03$; I 型绿泥石的 $\text{Al}^{\text{IV}}=0.76\sim 1.02$ 、 $\text{Al}^{\text{VI}}=0.89\sim 1.35$, II 型为 $\text{Al}^{\text{IV}}=0.97\sim 1.04$ 、 $\text{Al}^{\text{VI}}=1.00\sim 1.09$, III 型为 $\text{Al}^{\text{IV}}=0.83\sim 1.04$ 、 $\text{Al}^{\text{VI}}=0.88\sim 1.04$ 。在绿泥石特征分析时, 首先通过 Fe-Si 图解(图 7a; *a.p.f.u* 指原子数, 以 O=28 计算)对绿泥石成分进行分类, 然后使用 Zane and Weiss (1998) 图解确定绿泥石结构类型。绿泥石的 3 类样品数据多数落在了铁镁绿泥石区域(图 7b), 在 $\text{Al}+\square-\text{Mg}-\text{Fe}$ 三角图解中表现为富铁型特征。在 $\text{R}^{2+}-\text{Si}$ 图解中, 蒿坪沟 Ag-Au 多金属矿床矿区中 3 种类型绿泥石均落入了三八面体绿泥石区域, 并介于斜绿泥石和须腾石之间, 富镁铁而相对贫铝(图 7c)。



Chl—绿泥石; Ser—绢云母; Gn—方铅矿; Qz—石英; Sp—闪锌矿; Py—黄铁矿; Cal—一方解石

a—发育于石英脉两侧的绿泥石(正交偏光); b—隐爆角砾岩基质中填充的绿泥石(正交偏光); c—与黄铁矿、闪锌矿共生的绿泥石(正交偏光+反射光); d—填充在石英颗粒间隙的蠕虫状绿泥石(正交偏光); e—背散射镜下绿泥石电子探针打点位置分布, 可见绿泥石与绢云母共生; f—背散射镜下绿泥石电子探针打点位置分布

图 6 蒿坪沟 Ag-Au 多金属矿床绿泥石显微形态特征

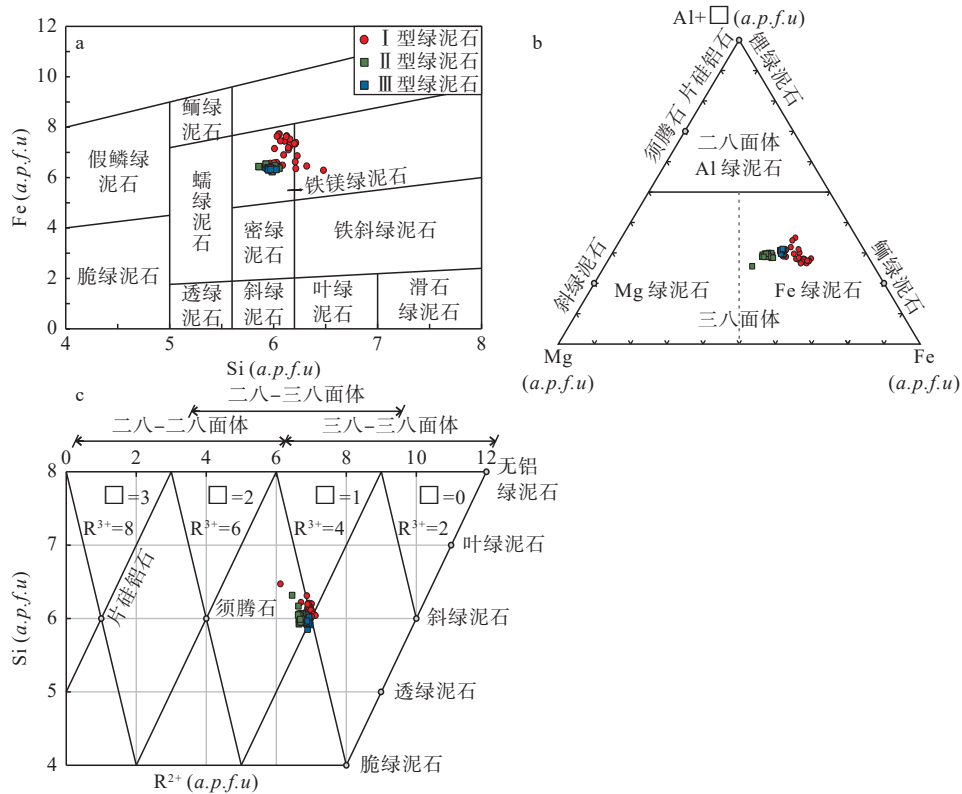
Fig. 6 Representative photomicrographs of chlorite characteristics of the Haopinggou Ag-Au polymetallic deposit

(a) Chlorite developed on both sides of quartz veins (cross-polarized light); (b) Chlorite filled in breccia matrix (cross-polarized light); (c) Chlorite coexisting with pyrite and sphalerite (cross-polarized light+ reflected light); (d) Worm-like chlorite filling the interstices of quartz grains (cross-polarized light); (e) Backscattered electron images of the distribution of chlorite EMPA dots, showing coexistence with sericite; (f) Backscattered electron images of the distribution of chlorite EMPA dots

Chl—chlorite; Ser—sericite; Gn—galena; Qz—quartz; Sp—sphalerite; Py—pyrite; Cal—calcite

绿泥石中的离子间相互置换普遍, 可能有 $\text{Fe}^{2+} \rightarrow \text{Mg}^{2+}$ 之间的任意替换, 契尔马克替代 Al^{IV} 与 $\text{Al}^{\text{VI}} \rightarrow \text{Si}(\text{Mg}^{2+}, \text{Fe}^{2+})$ 以及二八—三八面体 $3(\text{Mg}^{2+}, \text{Fe}^{2+}) \rightarrow \square + 2\text{Al}^{\text{VI}}$ (Inoue et al., 2009)。通常情况下, 在绿泥石结构晶格中, Si 和 Al^{IV} 占据四面体晶格,

$\text{Mg}^{2+}, \text{Fe}^{2+}$ 和 Al^{IV} 占据八面体位置。绿泥石在四面体和八面体位置上的替换关系通常通过 $\text{Al}^{\text{IV}}, \text{Al}^{\text{VI}}$ 和 $(\text{Fe}^{2+}, \text{Al}^{\text{VI}}) - \text{Mg}^{2+}$ 三者之间的相关关系图(图 8)来说明。 Al^{IV} 与 Al^{VI} 二者的相关性较差, 说明在 Al^{IV} 对 Si 原子的替换过程中, Al^{VI} 在八面体位置上对 Mg^{2+} 或



a—绿泥石 Fe-Si 图解(Deer et al., 1962); b—绿泥石 Al+□-Mg-Fe 图解(Zane and Weiss, 1998); c—绿泥石 Si-R²⁺图解(据刘燚平等, 2016 修改)

图 7 蒿坪沟 Ag-Au 多金属矿床绿泥石化学性质图解

Fig. 7 Chemical diagram of chlorite from the Haopinggou Ag-Au polymetallic deposit

(a) Fe vs. Si diagram of chlorite (Deer et al., 1962); (b) Al+□-Mg-Fe plot (Zane and Weiss, 1998); (c) Si vs. R²⁺ diagram (modified after Liu et al., 2016)

Fe²⁺的置换作用不明显(廖震等, 2010), 因此蒿坪沟 Ag-Au 多金属矿床中绿泥石 Al 与 Si 置换不属于单纯的钙镁闪石替代。Fe²⁺/(Fe²⁺+Mg²⁺)、Mg²⁺与 Al^{IV} 的正相关性不明显, 也再次印证了 Al^{VI} 在八面体位置上对 Mg²⁺和 Fe²⁺的置换较弱, 即不存在 Al^{VI}-Si 置换的时候同时发生了 Fe²⁺-Mg²⁺置换(Kranidiotis and Maclean, 1987)。

(Fe²⁺+Al^{VI})-Mg²⁺呈接近 1:1 的负相关关系, 说明绿泥石八面体位置主要发生了 Mg²⁺被 Fe²⁺+Al^{VI} 的置换, 而从 Fe²⁺和 Mg²⁺的相关关系图(图 8)可以看出, Fe²⁺和 Mg²⁺呈非常好的负相关线性关系, 方程为 Fe=-0.928Mg + 0.95 (决定系数 R²=0.764), 表明 Fe²⁺和 Mg²⁺的置换是绿泥石八面体位置上最重要的反应, Mg²⁺-Al^{IV} 相关性较差, 线性方程为 Mg²⁺=0.369 Al^{IV}-0.43 (决定系数 R²=0.14), 所以 Al^{VI} 对 Mg²⁺的置换不明显。蒿坪沟 Ag-Au 多金属矿床中的绿泥石仅表现 Fe²⁺对 Mg²⁺具有良好的线性关系, 而其他阳离子 Si⁴⁺与 Al^{VI} 均与 Mg²⁺相关性较差, 暗示了 3 种类型

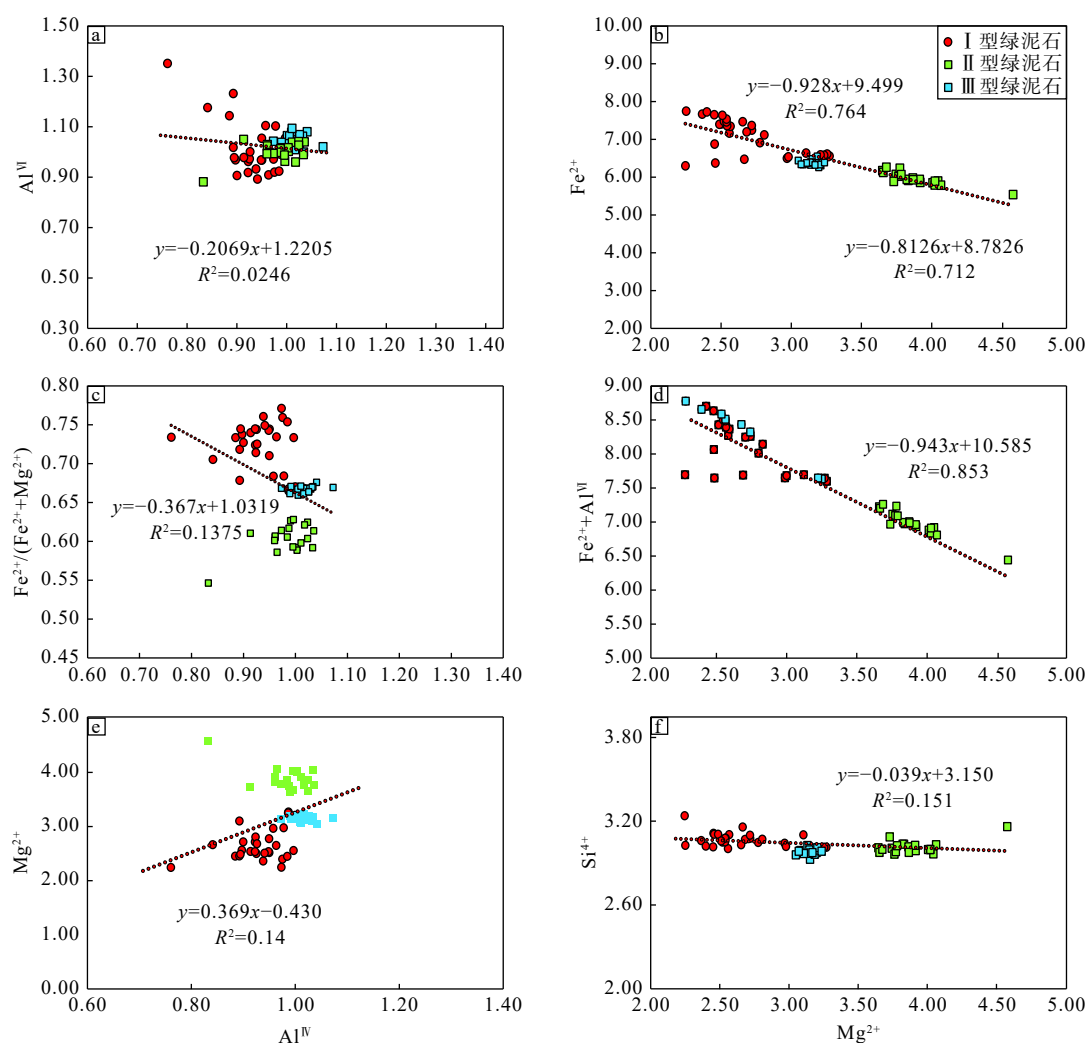
绿泥石可能具有不同的成因(Xie et al., 1997)。

Al/(Al+Mg+Fe)常被用来判别绿泥石与母岩之间的关系(Shirozu, 1978; Zane and Fyfe, 1995), 通常由镁铁质岩石形成的绿泥石具有较低的 Al/(Al+Mg+Fe)值(<0.35), 与泥质岩相关则比较高(>0.35)。I型、II型和III型绿泥石 Al/(Al+Mg+Fe) 小于 0.35, 显示均受镁铁质原岩控制, 该结果也与蒿坪沟 Ag-Au 铅锌矿床普遍发育的角闪岩和片麻岩围岩相符合。因此蒿坪沟 Ag-Au 多金属矿床的绿泥石中 Fe 元素的来源可能是镁铁质围岩或者含矿流体。

5 讨论

5.1 绿泥石形成温度

绿泥石成分多变, 对环境极其敏感, 通过其成分和结构的规律性变化来反演温度已经得到了广泛应用(Kranidiotis and Maclean, 1987; Zane and Fyfe,



a—绿泥石 Al^{IV}-Al^{IV}图解; b—绿泥石 Fe²⁺-Mg²⁺图解; c—绿泥石 Fe^{2+/(Fe²⁺+Mg²⁺)}-Al^{IV}图解; d—绿泥石 (Fe^{2+ + Al^{IV})}-Mg²⁺图解; e—绿泥石 Mg²⁺-Al^{IV}图解; f—绿泥石 Si⁴⁺-Mg²⁺图解

图 8 蒿坪沟 Au-Ag 多金属矿床绿泥石阳离子相关关系图 (单位为 a.p.f.u)

Fig. 8 Correlation of cations in chlorites from the Haopinggou Ag-Au polymetallic deposit(unit a.p.f.u)

(a) Al^{IV} vs. Al^{IV} diagram of chlorite; (b) Fe²⁺ vs. Mg²⁺ diagram of chlorite; (c) Fe^{2+/(Fe²⁺+Mg²⁺)} vs. Al^{IV} diagram of chlorite; (d) (Fe^{2+ + Al^{IV})} vs. Mg²⁺ diagram of chlorite; (e) Mg²⁺ vs. Al^{IV} diagram of chlorite; (f) Si⁴⁺ vs. Mg²⁺ diagram of chlorite

1995; Inoue et al., 2009; 刘燚平等, 2016; Zhang et al., 2022)。Cathelineau and Nieva(1985)利用绿泥石中的Al^{IV}与温度之间的正相关性提出了绿泥石固溶体地质温度计;之后 Kranidiotis and Maclean(1987)进一步修正了该温度计,并强调该地质温度计适用于铝饱和条件。Jowett(1991)则进一步限定适用的前提为150~325 °C的热液条件。蒿坪沟Ag-Au多金属矿床中3种类型绿泥石的Fe/(Fe+Mg)的范围为0.55~0.74,其中Al₂O₃含量为13.23%~17.61%,在显微镜下可见绿泥石与石英、铁白云石共生,且各类绿泥石都基本伴有绢云母化(图6e~f),所以可认为其处于一个铝饱和的环境,符合绿泥石地质温度计

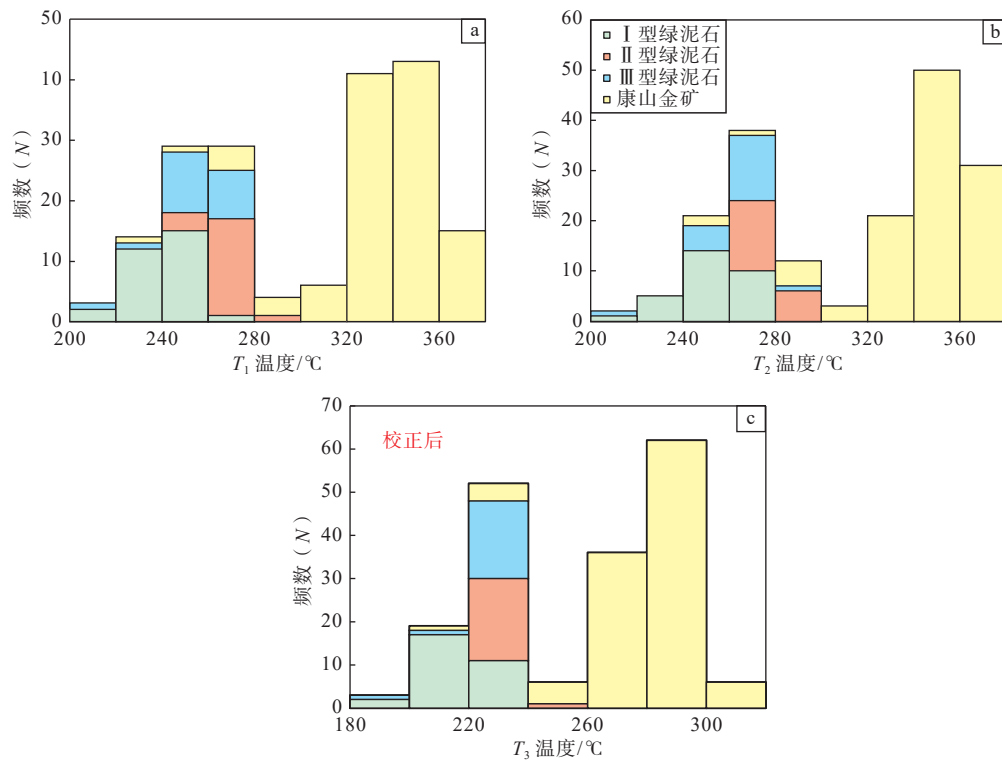
的使用范围。由于绿泥石形成环境的复杂性,为探讨地质温度计在蒿坪沟Ag-Au多金属矿床中的适用性,文章使用Cathelineau(1988)提出的温度公式(1)计算出T₁,然后使用Jowett(1991)提出的修正公式(2)计算出T₂,

$$T_1 = 321.98 \times Al^{IV} - 61.92 \quad (1)$$

$$T_2 = 318.5 \times (Al^{IV} + 0.10[Fe/(Fe + Mg)]) - 68.7 \quad (2)$$

3种类型绿泥石的温度频数直方图如图9所示。

根据绿泥石形成温度频数分布直方图可知(图9a、9b),T₁整体结果较T₂偏小,每个点相差的温度范围在9~15 °C之间。用T₁与T₂的平均值T_{平均}来评估



a—绿泥石形成温度 T_1 频数分布直方图; b—绿泥石形成温度 T_2 频数分布直方图; c—绿泥石形成温度 T_3 频数分布直方图

图 9 蒿坪沟 Ag-Au 多金属矿床绿泥石形成温度频数 (N) 分布直方图

Fig. 9 Hsitogram of formation temperatures of chlorites from the Haopinggou Ag-Au polymetallic deposit

(a) Hsitogram of formation T_1 of chlorites; (b) Hsitogram of formation T_2 of chlorites; Hsitogram of formation T_3 of chlorites

铅锌成矿阶段中热液的流体温度, 结果表明 $T_{\text{平均}}$ 相较于已有研究使用流体包裹体等方式获得的温度整体偏高, 误差较大。如 Zhang et al (2020) 通过流体包裹体获得了昆山金成矿期的温度 (226~305 °C), 以及矿田内与蒿坪沟 Ag-Au 多金属矿床临近矿床的铅锌硫化物成矿期的温度 (170~270 °C; Li et al., 2013; 徐进鸿, 2021) 都低于相应的 $T_{\text{平均}}$ 。

绿泥石中 Al^{IV} 与温度有着密切的关系, 但也会随着环境中 $\text{Fe}/(\text{Fe}+\text{Mg})$ 的升高而变化 (Zane and Fyfe, 1995)。为了消除 $\text{Fe}/(\text{Fe}+\text{Mg})$ 对温度的影响, 可以利用公式(3)对绿泥石 Al^{IV} 进行校正 (周栋等, 2018):

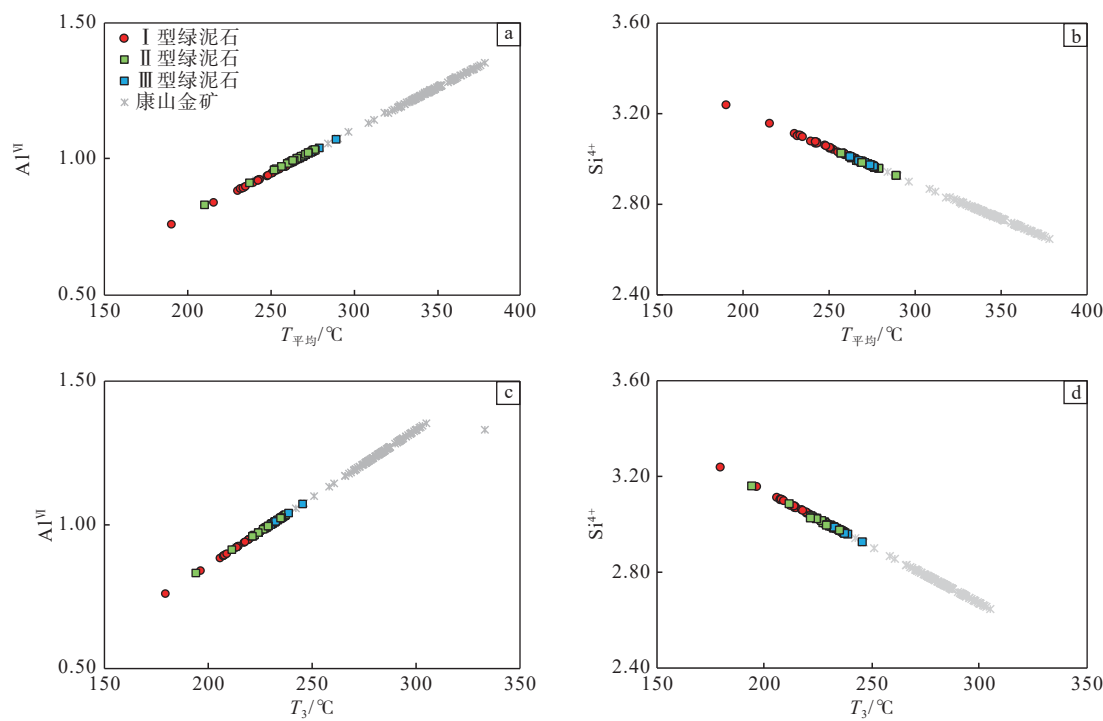
$$\text{Al}_{\text{校正}}^{\text{IV}} = \text{Al}_{\text{计算}} + 0.0268 (\text{Fe}/\text{Fe} + \text{Mg} - 0.65) \quad (3)$$

$$T_3 = 106.2 \text{Al}_{\text{校正}}^{\text{IV}} + 17.5 \quad (4)$$

然后使用公式(4)计算校正后的温度 T_3 , 结果见图 9c。校正后的温度 T_3 与已有成果获得对应期次的成矿流体温度在同一范围内, 印证了 T_3 的可信度, 因此 T_3 可以代表该矿床中绿泥石的形成温度。结果表明, 蒿坪沟 Ag-Au 多金属矿床校正后的 II 型

绿泥石温度范围为 224~245 °C, 平均温度为 233 °C; III 型绿泥石比前者稍低, 温度范围为 (194~237 °C), 平均为 226 °C; I 型绿泥石的温度最低, 范围为 179~227 °C, 平均 216 °C。II、III 类绿泥石伴生于石英-铅锌硫化物 (图 6b—6d), 而 I 类绿泥石形成于热液对围岩的改造。形成机制的不同可能造成了 II、III 类绿泥石与 I 类的温度差异。虽然 3 种类型绿泥石形成温度存在差异, 但总体上相差不大, 也暗示了该期热液活动较为稳定, 没有经历多期次热液-变质活动的叠加改造, 与绿泥石的广泛发育可能指示存在一定规模的铅锌成矿相吻合。

绿泥石中的阳离子个数与温度之间显示出较好的线性相关关系 (图 10)。Cathelineau (1988) 认为在 100~350 °C 内, 温度与绿泥石 Al^{IV} 值呈正相关关系, 而与八面体空位和 Al^{VI} 呈负相关关系。蒿坪沟 Ag-Au 多金属矿床中的绿泥石形成温度 $T_{\text{平均}}$ 与 Al^{VI} 及 Si^{4+} 的关系图解指示了良好的线性关系 (图 10a、10b), 同样校正后的温度 T_3 与 Al^{VI} 及 Si^{4+} 的关系表现出了明显的线性相关性 (图 10c、10d), 该结果与其他学者在地热系统中对绿泥石的研究结果相似, 证



a—绿泥石 Al^{IV} - $T_{\text{平均}}$ 关系图解; b—绿泥石 Si^{4+} - $T_{\text{平均}}$ 关系图解; c—绿泥石 Al^{IV} - T_3 关系图解; d—绿泥石 Si^{4+} - T_3 关系图解

图 10 绿泥石形成温度 T 与 Al^{IV} 及 Si^{4+} 相关性图解

Fig. 10 Correlation diagram of T vs. Al^{IV} and Si^{4+}

(a) Al^{IV} vs. T_{average} diagram of chlorite; (b) Si^{4+} vs. T_{average} diagram of chlorite; (c) Al^{IV} vs. T_3 diagram of chlorite; (d) Si^{4+} vs. T_3 diagram of chlorite

实了该温度体系的适用性(图 10; 周栋等, 2018; 张娟等, 2021)。

5.2 成矿流体性质

绿泥石的形成过程受水-岩反应控制(廖震, 2010), 从热液体系中析出时, 其化学组成受宿主岩性、流体的复杂成分以及物理化学条件影响(Zhang et al., 2022)。在温度条件相近的中-低温热液矿床的形成过程中, 成矿流体的 pH 值对元素的迁移过程有明显的影响。如 pH 值较小, 则酸性组分更容易对碱性组分发生取代作用, 即发生 Fe 对 Mg 的取代, 反之若 Mg 取代 Fe, 则表征相对碱性的环境(张娟等, 2021)。I、II、III型绿泥石的 $\text{Fe}/(\text{Fe}+\text{Mg})$ 值较高, 分别为 0.67~0.76、0.66~0.67、0.59~0.63, 说明 3 种类型绿泥石均形成于相对酸性的还原环境中。酸性的环境也有利于水-岩反应的相互作用, 促进了围岩的溶解, 为金属硫化物的进一步沉淀提供空间(Li et al., 2013)。该过程也产生了泥质的蚀变矿物, 如蒿坪沟 Ag-Au 多金属矿脉周围绿泥石化和硅化发生的部位常被泥化覆盖, 其形成于酸性流体对围岩中钾质矿物的萃取(Fialips et al., 1998; Reyes, 1990)。

5.3 绿泥石形成机制及其找矿意义

绿泥石是岩浆热液矿床成矿机制及找矿勘查的重要指示物。对于斑岩相关的 Cu(Au-Mo)矿床, 可以通过微量元素的变化趋势指示热液中心(Dora and Randive, 2015; Wilkinson et al., 2015; 葛祥坤等, 2020), 典型的如中国土屋-延东斑岩型铜矿床(Xiao et al., 2018a, 2018b)通过 V 和 Ti 含量特征来示踪热液中心。而对于浅成中-低温热液矿床, 绿泥石广泛发育于主成矿期(周栋等, 2018; Zhang et al., 2020; 张娟等, 2021), 并为成矿元素的沉淀提供了有利条件(李占轲等, 2010; 张娟等, 2021)。蒿坪沟 Ag-Au 多金属矿床内共识别出 3 种类型的绿泥石, 其形成机制的厘定对探讨成矿过程及对开展找矿预测尤为重要。

蒿坪沟 Ag-Au 多金属矿床成矿过程中大量含铁碳酸盐(菱铁矿、铁白云石)的出现指示了富含 Fe 的成矿热液(Li et al., 2013)。含 Fe 热液与镁铁质围岩强烈的相互作用导致了矿区富铁绿泥石的产生(图 7)。根据其产出部位及矿物组合特征, 现对蒿坪沟 Ag-Au 多金属矿床 3 种类型的富铁绿泥石形成机制进行分析。

(1) I 型绿泥石为溶蚀-结晶。晚中生代热液

顺着北东向陡倾断裂向上运移, 同时与两侧的围岩发生了物理化学反应, 顺着片麻理或矿物间裂隙对片麻岩中的矿物(黑云母/角闪石)进行溶蚀交代(Li et al., 2013), 进而在围岩中形成绿泥石(杨献忠等, 2002; 李亮, 2011)。母矿物经常出现明显的蚀变特征, 全部/部分发生交代。这种情况形成的绿泥石发育于脉体两侧, 其中 Fe、Mg 组分多从围岩中获取。

(2) III型绿泥石为溶液-迁移-结晶。含矿热液携带溶蚀矿物(黑云母/角闪石)发生迁移, 随着物理化学条件变化在矿物间裂隙沉淀结晶形成绿泥石。该类绿泥石在裂隙内部分布均匀致密, 而向外延伸过程中常显示细脉状或蠕虫状分布的特征, 该情况下 Fe、Mg 组分主要为流体带入。

(3) II型绿泥石的形成过程可能介于前两者之间。岩浆的浅部就位过程中(Tian et al., 2023), 围岩由于流体沸腾作用形成隐爆角砾岩, 胶结物为孔隙度较大的岩粉和岩屑。之后成矿热液进入角砾岩, 充分溶蚀和交代胶结物, 在孔隙度较大、较为宽松的环境下形成细粒隐晶质绿泥石填充物。该情况下的 Fe、Mg 组分可能既来自母矿物, 也有流体的贡献。

结合绿泥石的形成机制可以还原银铅锌的成矿过程, 早期成矿流体进入断裂时由于 CO₂ 的释放导致溶液 pH 酸度的增加(Li et al., 2013), 酸性环境

有利于 Ag、Pb、Zn 离子的运移, 随后强烈的水-岩反应则会中和成矿流体中的酸性的 pH 值, pH 值的减小则会促进铅、锌等硫化物的沉淀(Li et al., 2013)。该过程发生于整个蒿坪沟 Ag-Au 多金属矿床银铅锌成矿事件中(高建京等, 2010; Li et al., 2013)。

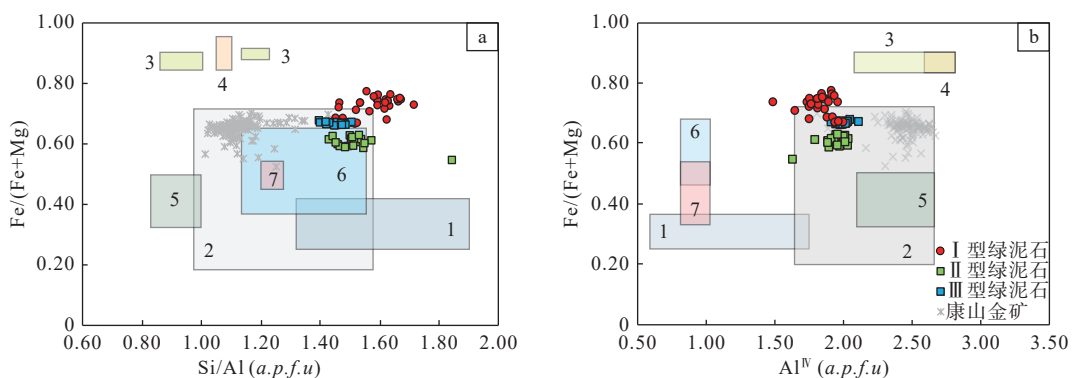
与蒿坪沟 Ag-Au 多金属矿床相比, 熊耳山矿集区康山金多金属矿床具有类似的成矿环境及流体特征(表 1, 图 11a、11b), 该矿床中 Au 形成于流体沸腾, 而流体混合导致 Ag、Pb、Zn 的沉淀(Zhang et al., 2020; 张哲铭等, 2023)。蒿坪沟 Ag-Au 多金属矿床中 I 型绿泥石来自大多落在了低温热液矿床区域外(图 11a、11b), 表明与矿化的关系相对较弱, II、III型绿泥石数据接近与花岗质侵入体主导的中-低温矿床范围(图 11a, Trumbull et al., 1996), 暗示了岩浆热液对成矿的重要意义。Tian et al.(2023)提出蒿坪沟 Ag-Au 多金属矿床中银铅锌成矿与~125 Ma 侵位花岗斑岩具有密切时空联系, 表明了成矿流体中的岩浆来源。矿区中的绿泥石与铅锌矿化关系密切, 与金矿化并无直接关系, 结合 Li et al. (2016)提出蒿坪沟 Ag-Au 多金属矿床 Au 和 Ag-Pb-Zn 来自不同的流体系统, 形成于两期独立的成矿事件, 因此推断蒿坪沟 Ag-Au 多金属矿床 Au 可能形成于更早的一期成矿事件中。

表 1 熊耳山矿集区蒿坪沟 Ag-Au 多金属矿床与康山金多金属矿床地质特征

Table 1 Geological characteristics of the Haopinggou Ag-Au polymetallic deposit and the Kangshan Au polymetallic deposit in the Xionger shan ore concentration area

矿床名称	蒿坪沟Ag-Au多金属矿床	康山金多金属矿床
矿床类型	岩浆热液型	岩浆热液型
大地构造位置	华北克拉通南缘、熊耳山矿集区西北部	华北克拉通南缘、熊耳山矿集区西南部
控矿构造	北东向陡倾断裂和局部隐爆角砾岩	北东向脆性断裂
成矿阶段及矿物组合(Li et al., 2013)	第一阶段: Qz-Sd-Mag-Elc 第二阶段: Gn-Sp-Qz-Ank 第三阶段: Qz-Cal-Fl —	第一阶段: Qz-Py 第二阶段: Qz-Py-Ccp-Au 第三阶段: Gn-Sp-gold-Qz-Ank- 第四阶段: Qz-Cal-Fl
成矿时代	热液独居石 125~123 Ma(Tian et al., 2023)	热液独居石年龄为 131 Ma(张哲铭等, 2023)
流体特征及来源	含银硫化物来自蒿坪沟花岗岩体, 表现为还原性的酸性流体(Li et al., 2016)	含金流体来自隐伏花岗岩体, 表现为相对弱酸性的还原环境; 其成矿机制为流体沸腾, 第三阶段主要成矿机制为流体混合(Zhang et al., 2020)
成矿温度(Li et al., 2013; 徐进鸿, 2021)	Qz-Sd-Mag-Elc: 217~349 °C Gn-Sp-Qz-Ank: 172~267 °C(194~237 °C) Qz-Cal-Fl: 116~205 °C	Qz-Py: 322~359 °C Qz-Py-Ccp-Au: 226~305 °C(256~302 °C) Gn-Sp-Au-Qz-Ank: 185~246 °C Qz-Cal-Fl: 130~221 °C
绿泥石分类	主要为铁镁绿泥石	富铁种属的绿泥石, 围岩属于铁镁绿泥石, 与矿化相关的绿泥石为铁绿泥石(周栎等, 2018)

注: 成矿温度为流体包裹体测温数据(Li et al., 2013; 徐进鸿, 2021), 括号内为绿泥石 EMPA 数据所计算出 T_g 温度



不同矿床类型中的绿泥石投图区域: 1—活动的地热系统; 2—块状硫化物矿床(Kranidiotis and Maclean, 1987); 3—热液铜(金)矿化带(Zane and Fyfe, 1995); 4—与铜金矿化相关的绿泥石(Dora and Randive, 2015); 5—云母石英岩中的绿泥石(Randive et al., 2015); 6—与花岗岩相关的矿床(Trumbull et al., 1996); 7—热液脉型矿床(Walshe, 1986)

a—绿泥石中 $\text{Fe}/(\text{Fe}+\text{Mg})$ — (Si/Al) 关系图解; b—绿泥石中 $\text{Fe}/(\text{Fe}+\text{Mg})$ — Al^{IV} 关系图解(据周栋等, 2018 修改)

图 11 不同成因类型矿床中的绿泥石特征

Fig. 11 Chlorite characteristics in different genetic types of deposits

(a) $\text{Fe}/(\text{Fe}+\text{Mg})$ vs. (Si/Al) diagram of chlorite; (b) $\text{Fe}/(\text{Fe}+\text{Mg})$ vs. Al^{IV} diagram of chlorite (modified after Zhou et al., 2018)

Data source: 1—active geothermal system; 2—massive sulfide deposit (Kranidiotis and Maclean, 1987); 3—hydrothermal mineralization zone (Zane and Fyfe, 1995); 4—Chlorites related to Cu-Au mineralization (Dora and Randive, 2015); 5—green-mica quartzites (Randive et al., 2015); 6—deposits associated with granite (Trumbull et al., 1996); 7—hydrothermal vein-type deposit (Walshe, 1986)

蒿坪沟 Ag-Au 多金属矿床从金成矿阶段、铅锌成矿阶段到碳酸盐阶段, 成矿环境和流体性质逐渐发生改变(Zhang et al., 2020; Tian et al., 2023)。在强烈的水-岩反应过程中, 镁铁质围岩中的斜长石和黑云母被蚀变为绢云母和绿泥石, 热液流体从围岩中获得了可观的 Fe^{2+} 、 Mg^{2+} 和 Ca^{2+} 等阳离子, 有利于碳酸盐矿物的沉淀。流体的 pH 由酸性逐渐变为弱酸性, 最后趋近于中性。低温流体(大气降水)的不断添加则导致成矿过程中温度逐渐下降(Li et al., 2013)。成矿环境及流体性质的差异也限制了金成矿与石英-碳酸盐阶段绿泥石的形成。

作为蒿坪沟 Au-Ag 多金属矿床内重要的热液蚀变产物, 绿泥石通常存在于矿化强烈的部位, 且 3 类绿泥石的野外识别标志都较为明显。Ⅱ型绿泥石在手标本下为墨绿色, 呈浸染状充填于基质中, 极易分辨; Ⅲ型绿泥石呈灰绿色充填于矿物间裂隙, 可以观察到较明显的矿物蚀变特征; Ⅰ型绿泥石通常发育于脉体两侧围岩, 本身不含矿, 但该类绿泥石的广泛发育可能是大规模含矿热液上涌与太华群片麻岩相互反应的结果, 在勘查过程中可以在蚀变围岩两侧寻找含矿石英脉体。

6 结论

蒿坪沟 Ag-Au 多金属矿床发育 3 种类型的绿

泥石, 其化学特征均反映了酸性、还原性的流体环境。3 种绿泥石发育于铅锌矿化强烈的部位, 可以作为铅锌矿脉的关键识别标志。绿泥石的形成与镁铁质围岩密切相关, 其化学性质暗示了早期成矿热液中有岩浆流体的参与。

(1) 蒿坪沟 Ag-Au 多金属矿床发育 3 种成因类型的绿泥石: I 型分布在石英脉两侧的围岩中, 由围岩蚀变形成; II 型呈细粒、隐晶质填充质隐爆角砾岩基质中; III 型与铅锌硫化物共生、以蠕虫状分布在矿物颗粒间隙。3 种类型的绿泥石均为斜绿泥石, 并落在了铁镁绿泥石的范围内, 在结构的阳离子置换中, 主要发生了 Fe^{2+} 对 Mg^{2+} 的置换, 其余置换作用均不明显。

(2) 矿区中与矿化相关的绿泥石形成温度略高于石英脉两侧的绿泥石, 运用绿泥石经验性公式计算该类矿床的温度时, 需要考虑 $\text{Fe}/(\text{Fe}+\text{Mg})$ 对温度的影响。

(3) 矿区中 3 种类型绿泥石的形成与镁铁质围岩密切相关, 形成机制可能包含溶蚀-结晶和溶蚀-迁移-结晶两种方式, 成矿流体为具有还原性的酸性富铁流体。

(4) 矿区中绿泥石通常存在于矿化强烈的部位, 代表强烈水-岩反应的发生, 其产生与大规模铅锌成矿期相匹配, 可以作为铅锌矿脉的关键识别标

志, 其化学性质暗示早期成矿热液中有岩浆流体参与。致谢: 在电子探针实验中得到了河北省区域地质调查院(河北省地学旅游研究中心)修迪的协助, 在数据处理方面得到了中国地质大学(北京)张伟博士的帮助; 同时感谢两位匿名审稿人以及主编提出的宝贵意见。

References

- BOURDELLE F, PARRA T, CHOPIN C, et al., 2013. A new chlorite geothermometer for diagenetic to low-grade metamorphic conditions[J]. *Contributions to Mineralogy and Petrology*, 165(4): 723-735.
- BOURDELLE F, CATHELINNEAU M, 2015. Low-temperature chlorite geo-thermometry: a graphical representation based on a $T\text{-}R^{2+}\text{-Si}$ diagram[J]. *European Journal of Mineralogy*, 27(5): 617-626.
- CATHELINNEAU M, NIEVA D, 1985. A chlorite solid solution geothermometer the Los Azufres (Mexico) geothermal system[J]. *Contributions to Mineralogy and Petrology*, 91(3): 235-244.
- CATHELINNEAU M, 1988. Cation site occupancy in chlorites and illites as a function of temperature[J]. *Clay Minerals*, 23(4): 471-485.
- CHEN Y J, SUI Y H, PIRAJNO F, 2003. Exclusive evidences for CMF model and a case of orogenic silver deposits: isotope geochemistry of the Tie-luping silver deposit, east Qinling orogen[J]. *Acta Petrologica Sinica*, 19(3): 551-568. (in Chinese with English abstract)
- CHEN Y J, PIRAJNO F, SUI Y H, 2004. Isotope geochemistry of the Tie-luping silver-lead deposit, Henan, China: a case study of orogenic silver-dominated deposits and related tectonic setting[J]. *Mineralium Deposita*, 39(5-6): 560-575.
- CHENG G G, 2013. Study on the mineralization and prognosis in western Mt. Xiong'er silver-lead-zinc deposit, Henan province[D]. Beijing: China University of Geosciences (Beijing). (in Chinese with English abstract)
- DAI C C, LIU X D, RAO Q, et al., 2017. Authigenic chlorite compositional evolution and temperature calculation of Xujiahe formation sandstone in central Sichuan basin[J]. *Geological Review*, 63(3): 831-841. (in Chinese with English abstract)
- DEER W A, HOWIE R A, ZUSSMAN J, 1962. Rock-forming minerals: sheet silicates[M]. London: Longman. 270.
- DIWU C R, SUN Y, ZHAO Y, et al., 2014. Geochronological, geochemical, and Nd-Hf isotopic studies of the Qinling complex, central China: implications for the evolutionary history of the North Qinling Orogenic Belt[J]. *Geoscience Frontiers*, 5(4): 499-513.
- DIWU C R, SUN Y, LIN C L, et al., 2017. Zircon U-Pb ages and Hf isotopes and their geological significance of Yiyang TTG gneisses from Henan province, China[J]. *Acta Petrologica Sinica*, 23(2): 253-262. (in Chinese with English abstract)
- DONG Y P, SAFONOVA I, WANG T, 2016. Tectonic evolution of the Qinling orogen and adjacent orogenic belts[J]. *Gondwana Research*, 30: 1-5.
- DORA M L, RANDIVE K R, 2015. Chloritisation along the Thanewasna shear zone, Western Bastar Craton, Central India: its genetic linkage to Cu-Au mineralisation[J]. *Ore Geology Reviews*, 70: 151-172.
- DYAR M D, GUIDOTTI C V, HARPER G D, et al., 1992. Controls on ferric iron in chlorite. *geological society of America*[J]. *Abstracts with Programs*, 24: 7.
- FANG W X, WANG L, LU J, et al., 2017. Chloritization facies and restoration of heat flux for tectonic-magmatic-thermal events of Sareke copper mine in the Xinjiang Uygur autonomous region, China[J]. *Acta Mineralogica Sinica*, 37(5): 661-675. (in Chinese with English abstract)
- FIALIPS C I, PETIT S, DECARREAU A, et al., 1998. Effects of temperature and PH on the kaolinite crystallinity[J]. *Mineralogical Magazine*, 62A(1): 452-453.
- GAO J J, MAO J W, YE H S, et al., 2010. Geology and ore-forming fluid of silver-lead-zinc lode deposit of Shagou, western Henan province[J]. *Acta Petrologica Sinica*, 26(3): 740-756. (in Chinese with English abstract)
- GE X K, JU H Y, ZHAO F H, et al., 2020. Characteristics of chlorites in the Shangdajing porphyry Mo deposit, Inner Mongolia and their metallogenetic implications[J]. *Geology and Exploration*, 56(4): 704-713. (in Chinese with English abstract)
- HAN J S, YAO J M, CHEN H Y, et al., 2014. Fluid inclusion and stable isotope study of the Shagou Ag-Pb-Zn deposit, Luoning, Henan province, China: Implications for the genesis of an orogenic lode Ag-Pb-Zn system[J]. *Ore Geology Reviews*, 62: 199-210.
- HAN Y G, ZHANG S H, PIRAJNO F, et al., 2009. New ${}^{40}\text{Ar}$ - ${}^{39}\text{Ar}$ age constraints on the deformation along the Machaoying fault zone: Implications for Early Cambrian tectonism in the North China Craton[J]. *Gondwana Research*, 16(2): 255-263.
- HEDENQUIST J W, ANTONIO ARRIBAS S, GONZALEZ-URIEN E, 2000. Exploration for epithermal gold deposits[M]//HAGEMANN S G, BROWN P E. *Reviews in economic geology*. Littleton: Society of Economic Geologists. 245-277.
- HILLIER S, 1993. Origin, diagenesis, and mineralogy of chlorite minerals in Devonian lacustrine Mudrocks, Orcadian basin, Scotland[J]. *Clays and Clay Minerals*, 41(2): 240-259.
- HU X K, TANG L, ZHANG S T, et al., 2020. Geochemistry, zircon U-Pb geochronology and Hf-O isotopes of the Late Mesozoic granitoids from the Xiong'ershan area, East Qinling Orogen, China: implications for petrogenesis and molybdenum metallogenesis[J]. *Ore Geology Reviews*, 124: 103653.
- INOUE A, 1995. Formation of clay minerals in hydrothermal environments[M]//VELDE B. *Origin and mineralogy of clays: clays and the environment*. Berlin: Springer. 268-329.
- INOUE A, MEUNIER A, PATRIER-MAS P, et al., 2009. Application of chemical geothermometry to low-temperature trioctahedral chlorites[J]. *Clays and Clay Minerals*, 57(3): 371-382.
- JOWETT E C, 1991. Fitting iron and magnesium into the hydrothermal chlorite geothermometer[M]. GAC/MAC/SEG Joint annual meeting. Toronto: 27-29, , Program with Abstracts 16: A62.
- KRANIDOTIS P, MACLEAN W H, 1987. Systematics of chlorite alteration at the Phelps Dodge massive sulfide deposit, Matagami, Quebec[J]. *Economic Geology*, 82(7): 1898-1911.
- LAIRD J, 1988. Chlorites: metamorphic petrology[J]. *Reviews in Mineralogy and Geochemistry*, 19(1): 405-453.
- LI H M, WANG D H, WANG X X, et al., 2012. The Early Mesozoic synecraton granite in Xiong'er Mountain area, southern margin of North China

- Craton: SHRIMP zircon U-Pb dating, geochemistry and its significance[J]. *Acta Petrologica et Mineralogica*, 31(6): 771-782. (in Chinese with English abstract)
- LI L, 2011. Study of characters of biotite and chlorite of molybdenum deposit in Antuoling, Hebei[D]. Beijing: China University of Geosciences (Beijing). (in Chinese with English abstract)
- LI L X, LI H M, XU Y X, et al., 2015. Zircon growth and ages of migmatites in the Algoma-type BIF-hosted iron deposits in Qianxi Group from eastern Hebei province, China: timing of BIF deposition and anatexis[J]. *Journal of Asian Earth Sciences*, 113: 1017-1034.
- LI N, SUN Y L, LI J, et al., 2008. Molybdenite Re-Os isotope age of the Dahu Au-Mo deposit, Xiaoqinling and the Indosinian mineralization[J]. *Acta Petrologica Sinica*, 24(4): 810-816. (in Chinese with English abstract)
- LI N, CHEN Y J, SANTOSH M, et al., 2018. Late Mesozoic granitoids in the Qinling Orogen, Central China, and tectonic significance[J]. *Earth-Science Reviews*, 182: 141-173.
- LI Z K, LI J W, CHEN L, et al., 2010. Occurrence of silver in the Shagou Ag-Pb-Zn Deposit, Luoning County, Henan province: implications for mechanism of silver enrichment[J]. *Earth Science: Journal of China University of Geosciences*, 35(4): 621-636. (in Chinese with English abstract)
- LI Z K, LI J W, ZHAO X F, et al., 2013. Crustal-extension Ag-Pb-Zn veins in the Xiong'ershan District, Southern North China craton: constraints from the Shagou deposit[J]. *Economic Geology*, 108(7): 1703-1729.
- LI Z K, LI J W, COOKE D R, et al., 2016. Textures, trace elements, and Pb isotopes of sulfides from the Haopinggou vein deposit, southern North China Craton: implications for discrete Au and Ag-Pb-Zn mineralization[J]. *Contributions to Mineralogy and Petrology*, 171(12): 99.
- LIANG T, LU R, LUO Z H, et al., 2015. LA-ICP-MS U-Pb age of zircons from Haopinggou Biotite granite porphyry in Xiong'er Mountain, Western Henan province, and its geologic implications[J]. *Geological Review*, 61(4): 901-912. (in Chinese with English abstract)
- LIAO Z, LIU Y P, LI C Y, et al., 2010. Characteristics of chlorites from Du-long Sn-Zn deposit and their metallogenetic implications[J]. *Mineral Deposits*, 29(1): 169-176. (in Chinese with English abstract)
- LIU W Y, LIU J S, HE M X, et al., 2019. Petrogeochemistry, zircon U-Pb ages and Hf isotopic composition of Haopinggou pluton, Western Henan[J]. *The Chinese Journal of Nonferrous Metals*, 29(7): 1551-1566. (in Chinese with English abstract)
- LIU Y P, ZHANG S Y, ZHANG H F, 2016. Advances on mineral genesis of chlorite: a review[J]. *Advances in Geosciences*, 6(3): 264-282. (in Chinese with English abstract)
- LOWELL J D, GUILBERT J M, 1970. Lateral and vertical alteration-mineralization zoning in porphyry ore deposits[J]. *Economic Geology*, 65(4): 373-408.
- LYU Z C, CHEN H, MI K F, et al., 2022. The theory and method of ore prospecting prediction for exploration area: case studies of the Lala copper deposit in Sichuan, Muhu-Maerkantu manganese ore deposit in Xinjiang and Aonaodaba tin-polymetallic deposit in Inner Mongolia[J]. *Journal of Geomechanics*, 28(5): 842-865. (in Chinese with English abstract)
- MAO J W, ZHENG R F, YE H S, et al., 2006. $^{40}\text{Ar}/^{39}\text{Ar}$ dating of fuchsite and sericite from altered rocks close to ore veins in Shagou large-size Ag-Pb-Zn deposit of Xiong'ershan area, western Henan province, and its significance[J]. *Mineral Deposits*, 25(4): 359-368. (in Chinese with English abstract)
- MAO J W, YE H S, WANG R T, et al., 2009. Mineral deposit model of Mesozoic porphyry Mo and vein-type Pb-Zn-Ag ore deposits in the eastern Qinling, Central China and its implication for prospecting[J]. *Geological Bulletin of China*, 28(1): 72-79. (in Chinese with English abstract)
- MAO J W, XIE G Q, PIRAJNO F, et al., 2010. Late Jurassic-Early Cretaceous granitoid magmatism in Eastern Qinling, central-eastern China: SHRIMP zircon U-Pb ages and tectonic implications[J]. *Australian Journal of Earth Sciences*, 57(1): 51-78.
- MAO J W, PIRAJNO F, COOK N, 2011. Mesozoic metallogeny in East China and corresponding geodynamic settings—An introduction to the special issue[J]. *Ore Geology Reviews*, 43(1): 1-7.
- PACEY A, WILKINSON J J, COOKE D R, 2020. Chlorite and epidote mineral chemistry in porphyry ore systems: a case study of the Northparkes District, New South Wales, Australia[J]. *Economic Geology*, 115(4): 701-727.
- RANDIVE K R, KORAKOPPA M M, MULEY S V, et al., 2015. Paragenesis of Cr-rich muscovite and chlorite in green-mica quartzites of Saigaon-Palasaon area, Western Bastar Craton, India[J]. *Journal of Earth System Science*, 124(1): 213-225.
- REYES A G, 1990. Petrology of Philippine geothermal systems and the application of alteration mineralogy to their assessment[J]. *Journal of Volcanology and Geothermal Research*, 43(1-4): 279-309.
- SHIROZU H, 1978. Chlorite minerals[J]. *Developments in Sedimentology*, 26: 243-264.
- SILLITOE R H, HEDENQUIST J W, 2005. Linkages between volcanotectonic settings, ore-fluid compositions, and epithermal precious metal deposits[M]//SIMMONS S F, GRAHAM I. *Volcanic, geothermal, and ore-forming fluids: rulers and witnesses of processes within the earth*. Littleton: Society of Economic Geologists: 315-343.
- TANG K F, 2014. Characteristics, genesis, and geodynamic setting of representative gold deposits in the Xiong'ershan district, southern margin of the North China Craton[D]. Wuhan: China University of Geosciences. (in Chinese with English abstract)
- TIAN Y F, MAO J W., JIAN W, et al., 2023. Recognition of the Xiayu intermediate-sulfidation epithermal Ag-Pb-Zn-Au(-Cu) mineralization in the East Qinling polymetallic ore belt, China: constraints from geology and geochronology[J]. *Ore Geology Reviews*, 156: 105398.
- TRUMBULL R B, HUA L, LEHRBERGER G, et al., 1996. Granitoid-hosted gold deposits in the Anjiayingzi district of inner Mongolia, People's Republic of China[J]. *Economic Geology*, 91(5): 875-895.
- WALSHE J L, 1986. A six-component chlorite solid solution model and the conditions of chlorite formation in hydrothermal and geothermal systems[J]. *Economic Geology*, 81(3): 681-703.
- WANG C M, DENG J, BAGAS L, et al., 2021. Origin and classification of the Late Triassic Huashuping gold deposit in the eastern part of the Qinling-Dabie Orogen, China: implications for gold metallogeny[J]. *Mineralium Deposita*, 56(4): 725-742.
- WANG J L, ZHANG H F, ZHANG J, et al., 2020. Highly heterogeneous Pb isotope composition in the Archean continental lower crust: insights from the high-grade metamorphic suite of the Taihua Group, Southern North

- China Craton[J]. *Precambrian Research*, 350: 105927.
- WANG X L, JIANG S Y, DAI B Z, 2010. Melting of enriched Archean sub-continental lithospheric mantle: evidence from the ca. 1760 Ma volcanic rocks of the Xiong'er Group, southern margin of the North China Craton[J]. *Precambrian Research*, 182(3): 204-216.
- WANG X X, WANG T, KE C H, et al., 2015. Nd-Hf isotopic mapping of Late Mesozoic granitoids in the East Qinling orogen, central China: constraint on the basements of terranes and distribution of Mo mineralization[J]. *Journal of Asian Earth Sciences*, 103: 169-183.
- WANG X Y, MAO J W, CHENG Y B, et al., 2014. Characteristics of chlorite from the Xinliaodong Cu polymetallic deposit in eastern Guangdong province and their geological significance[J]. *Acta Petrologica et Mineralogica*, 33(5): 885-905. (in Chinese with English abstract)
- WILKINSON J J, CHANG Z S, COOKE R D, et al., 2015. The chlorite proximitator: a new tool for detecting porphyry ore deposits[J]. *Journal of Geochemical Exploration*, 152: 10-26.
- XIAO B, CHEN H Y, HOLLINGS P, et al., 2018a. Element transport and enrichment during propylitic alteration in Paleozoic porphyry Cu mineralization systems: insights from chlorite chemistry[J]. *Ore Geology Reviews*, 102: 437-448.
- XIAO B, CHEN H Y, WANG Y F, et al., 2018b. Chlorite and epidote chemistry of the Yandong Cu deposit, NW China: metallogenetic and exploration implications for Paleozoic porphyry Cu systems in the Eastern Tianshan[J]. *Ore Geology Reviews*, 100: 168-182.
- XIE X G, BYERLY G R, FERRELL JR E, 1997. Iib trioctahedral chlorite from the Barberton greenstone belt: crystal structure and rock composition constraints with implications to geothermometry[J]. *Contributions to Mineralogy and Petrology*, 126(3): 275-291.
- XU J H, 2021. Deposit characteristics and metallogenesis of thin vein-type hydrothermal silver-lead-zinc deposits in the Xiong'ershan district along the eastern Qinling orogenic belt[D]. Beijing: University of Chinese Academy of Sciences.
- YANG F, XUE F, Santosh M, et al., 2019. Late Mesozoic magmatism in the East Qinling Orogen, China and its tectonic implications[J]. *Geoscience Frontiers*, 10(5): 1803-1821.
- YANG X Z, YANG Z L, TAO K Y, et al., 2002. Formation temperature of chlorite in oil-bearing basalt[J]. *Acta Mineralogica Sinica*, 22(4): 365-370. (in Chinese with English abstract)
- YE H S, 2006. The mesozoic tectonic evolution and Pb-Zn-Ag Metallogeny in the south margin of North China craton[J]. Beijing: Chinese Academy of Geological Sciences. (in Chinese with English abstract)
- YUAN H, HAN R S, FENG Z X, et al., 2022. Mineralization-alteration zoning law and element compositional zoning pattern in mineralized altered rocks from the Daliangzi Pb-Zn deposit, southwestern Sichuan[J]. *Journal of Geomechanics*, 28(3): 432-447. (in Chinese with English abstract)
- ZANE A, WEISS Z, 1998. A procedure for classifying rock-forming chlorites based on microprobe data: una procedura per la classificazione delle cloriti sulla base di dati microchimici[J]. *Rendiconti Lincei*, 9(1): 51-56.
- ZANE W, FYFE W S, 1995. Chloritization of the hydrothermally altered bedrock at the Igarapé Bahia gold deposit, Carajás, Brazil[J]. *Mineralium Deposita*, 30(1): 30-38.
- ZHANG G W, GUO A L, DONG Y P, et al., 2019. Rethinking of the Qinling orogen[J]. *Journal of Geomechanics*, 25(5): 746-768. (in Chinese with English abstract)
- ZHANG J, LIU X X, WANG Y T, et al., 2021. Characteristics of chlorite from the Baguamiao gold deposit in Shaanxi province and its geological implication[J]. *Geological Bulletin of China*, 40(4): 586-603. (in Chinese with English abstract)
- ZHANG W, ZHANG F F, WANG Y H, et al., 2022. Chlorite chemistry, H-O-S-Pb isotopes and fluid characteristics of the Yuhai Cu-Mo Deposit in Eastern Tianshan: implications for porphyry copper mineralization and exploration[J]. *Journal of Geochemical Exploration*, 241: 107059.
- ZHANG X M, ZHANG D, BI M F, et al., 2021. Genesis and geodynamic setting of the Nanyangtian tungsten deposit, SW China: Constraints from structural deformation, geochronology, and S-O isotope data[J]. *Ore Geology Reviews*, 138: 104354.
- ZHANG Y H, ZHANG S H, HAN Y G, et al., 2006. Strik-slip features of the machaoying fault zone and its evolution in the Huaxiong terrane, southern north China craton[J]. *Journal of Jilin University (Earth Science Edition)*, 36(2): 169-176, 193. (in Chinese with English abstract)
- ZHANG Z M, ZENG Q D, GUO Y P, et al., 2020. Genesis of the Kangshan Au-polymetallic deposit, Xiong'ershan District, North China Craton: Constraints from fluid inclusions and C-H-O-S-Pb isotopes[J]. *Ore Geology Reviews*, 127: 103815.
- ZHANG Z M, ZENG Q D, WANG Y B, et al., 2023. Metallogenetic age and fluid evolution of the Kangshan Au-polymetallic deposit in the southern margin of the North China Craton: constraints from monazite U-Pb age, and in-situ trace elements and S isotopes of pyrite[J]. *Acta Petrologica Sinica*, 39(3): 865-885. (in Chinese with English abstract)
- ZHAO G C, SUN M, WILDE S A, et al., 2005. Late Archean to Paleoproterozoic evolution of the North China Craton: key issues revisited[J]. *Precambrian Research*, 136(2): 177-202.
- ZHENG W, CHEN M H, ZHAO H J, et al., 2013. Skarn mineral characteristics of the Tiantang Cu-Pb-Zn polymetallic deposit in Guangdong province and their geological significance[J]. *Acta Petrologica et Mineralogica*, 32(1): 23-40. (in Chinese with English abstract)
- ZHOU D, ZHAO T P, ZHAO P B, et al., 2018. Chlorite EPMA characteristic and its geological significance of the Kangshan Au-Ag-Pb-Zn deposit in west of Henan[J]. *Mineral Exploration*, 9(5): 803-824. (in Chinese with English abstract)
- ZHOU J X, WANG X C, WILDE S A, et al., 2018. New insights into the metallogeny of MVT Zn-Pb deposits: a case study from the Nayongzhi in South China, using field data, fluid compositions, and in situ S-Pb isotopes[J]. *American Mineralogist*, 103(1): 91-108.
- ZOU S H, XU D R, DENG T, et al., 2019. Geochemical variations of the Late Mesozoic granitoids in the southern margin of North China Craton: A possible link to the tectonic transformation from compression to extension[J]. *Gondwana Research*, 75(0): 118-133.

附中文参考文献

- 陈衍景, 隋颖慧, PIRAJNO F, 2003. CMF 模式的排他性依据和造山型银矿实例: 东秦岭铁炉坪银矿同位素地球化学[J]. *岩石学报*, 19(3): 551-568.
- 程广国, 2013. 河南熊耳山西段银铅锌矿床成矿作用及找矿预测研

- 究 [D]. 北京: 中国地质大学(北京).
- 戴朝成, 刘晓东, 饶强, 等, 2017. 川中地区须家河组自生绿泥石成分演化及其形成温度计算 [J]. 地质论评, 63(3): 831-841.
- 第五春荣, 孙勇, 林慈銮, 等, 2007. 豫西宜阳地区 TTG 质片麻岩锆石 U-Pb 定年和 Hf 同位素地地质学 [J]. 岩石学报, 23(2): 253-262.
- 方维萱, 王磊, 鲁佳, 等, 2017. 新疆萨热克铜矿床绿泥石化变相与构造-岩浆-古地热事件的热通量恢复 [J]. 矿物学报, 37(5): 661-675.
- 高建京, 毛景文, 叶会寿, 等, 2010. 豫西沙沟脉状 Ag-Pb-Zn 矿床地质特征和成矿流体研究 [J]. 岩石学报, 26(3): 740-756.
- 葛祥坤, 句海玉, 赵峰华, 等, 2020. 内蒙古上打井斑岩型钼矿床绿泥石特征及成矿意义 [J]. 地质与勘探, 56(4): 704-713.
- 李亮, 2011. 河北省安妥岭辉钼矿黑云母、绿泥石特征研究 [D]. 北京: 中国地质大学(北京).
- 李诺, 孙亚莉, 李晶, 等, 2008. 小秦岭大湖金钼矿床辉钼矿铼锇同位素年龄及印支期成矿事件 [J]. 岩石学报, 24(4): 810-816.
- 李占轲, 李建威, 陈蕾, 等, 2010. 河南洛宁沙沟 Ag-Pb-Zn 矿床银的赋存状态及成矿机理 [J]. 地球科学: 中国地质大学学报, 35(4): 621-636.
- 梁涛, 卢仁, 罗照华, 等, 2015. 豫西熊耳山蒿坪沟黑云母花岗斑岩的锆石 LA-ICP-MSU-Pb 年龄及其地质意义 [J]. 地质论评, 61(4): 901-912.
- 廖震, 刘玉平, 李朝阳, 等, 2010. 都龙锡锌矿床绿泥石特征及其成矿意义 [J]. 矿床地质, 29(1): 169-176.
- 刘燚平, 张少颖, 张华锋, 2016. 绿泥石的成因矿物学研究综述 [J]. 地球科学前沿, 6(3): 264-282.
- 刘文毅, 刘继顺, 何美香, 等, 2019. 豫西蒿坪沟岩体岩石地球化学、锆石 U-Pb 年龄及 Hf 同位素组成 [J]. 中国有色金属学报, 29(7): 1551-1566.
- 吕志成, 陈辉, 毅奎峰, 等, 2022. 勘查区找矿预测理论与方法及其应用案例 [J]. 地质力学学报, 28(5): 842-865.
- 毛景文, 郑榕芬, 叶会寿, 等, 2006. 豫西熊耳山地区沙沟银铅锌矿床成矿的 ^{40}Ar - ^{39}Ar 年龄及其地质意义 [J]. 矿床地质, 25(4): 359-368.
- 毛景文, 叶会寿, 王瑞廷, 等, 2009. 东秦岭中生代钼铅锌银多金属矿床模型及其找矿评价 [J]. 地质通报, 28(1): 72-79.
- 唐克非, 2014. 华北克拉通南缘熊耳山地区金矿床时空演化、矿床成因及成矿构造背景 [D]. 武汉: 中国地质大学(武汉).
- 王小雨, 毛景文, 程彦博, 等, 2014. 粤东新寮岽铜多金属矿床绿泥石特征及其地质意义 [J]. 岩石矿物学杂志, 33(5): 885-905.
- 徐进鸿, 2021. 东秦岭熊耳山地区薄脉状热液型 Ag-Pb-Zn 矿床特征与成矿作用研究 [D]. 北京: 中国科学院大学.
- 杨献忠, 杨祝良, 陶奎元, 等, 2002. 含油玄武岩中绿泥石的形成温度 [J]. 矿物学报, 22(4): 365-370.
- 叶会寿, 2006. 华北陆块南缘中生代构造演化与铅锌银成矿作用 [D]. 北京: 中国地质科学院.
- 袁航, 韩润生, 冯志兴, 等, 2022. 川西南大梁子铅锌矿床矿化蚀变分带规律与元素组合分带模型 [J]. 地质力学学报, 28(3): 432-447.
- 张国伟, 郭安林, 董云鹏, 等, 2019. 关于秦岭造山带 [J]. 地质力学学报, 25(5): 746-768.
- 张娟, 刘新星, 王义天, 等, 2021. 陕西凤太矿集区八卦庙金矿床绿泥石特征及其找矿意义 [J]. 地质通报, 40(4): 586-603.
- 张元厚, 张世红, 韩以贵, 等, 2006. 华熊地块马超营断裂走滑特征及演化 [J]. 吉林大学学报(地球科学版), 36(2): 169-176, 193.
- 张哲铭, 曾庆栋, 王永彬, 等, 2023. 华北克拉通南缘康山金多金属矿床成矿时代及流体演化: 来自独居石 U-Pb 年龄、黄铁矿微量元素和原位 S 同位素制约 [J]. 岩石学报, 39(3): 865-885.
- 郑伟, 陈懋弘, 赵海杰, 等, 2013. 广东省天堂铜铅锌多金属矿床矽卡岩矿物学特征及其地质意义 [J]. 岩石矿物学杂志, 32(1): 23-40.
- 周栋, 赵太平, 赵鹏彬, 等, 2018. 豫西康山金银铅锌矿床绿泥石电子探针成分特征及其地质意义 [J]. 矿产勘查, 9(5): 803-824.

开放科学 (资源服务) 标识码 (OSID) :

可扫码直接下载文章电子版, 也有可能听到作者的语音介绍及更多文章相关资讯

